J FODEN

THE RATHJEN GNEISS: CONSTRAINTS ON THE TECTONIC HISTORY OF THE KANMANTOO GROUP AROUND SPRINGTON, SOUTH AUSTRALIA.

by

Tania L.A. Madigan

Thesis submitted as partial fulfilment for the Honours Degree of Bachelor of Arts

Department of Geology,
University of Adelaide,
November 1988.

TABLE OF CONTENTS

LIST OF TABLES, FIGURES AND PLATES

A. Tables

B. Figures

C. Plates

ABSTRACT

The Rathjen gneiss in the vicinity of Springton in the Mount Lofty Ranges is shown to be fundamentally important to our understanding of the metamorphic and deformational history of the Southern Adelaide Foldbelt. Field and geochemical criteria are used to prove conclusively that the Rathjen gneiss is a metamorphosed intrusive. A prominent N-S trending stretching lineation particularly well developed in the Rathjen gneiss indicates previously unrecognized N-S tectonic transport early in the history of the Delamerian Orogeny. Amphibole-plagioclase equilibria in the mapped area indicate metamorphic conditions (~700°C, < 5 kbars) consistent with the results of studies in nearby areas (e.g. Sandiford et al., in press), although the errors associated with these constraints are large and therefore the comparison tenuous. These temperatures are clearly in excess of those expected to be reached by crustal thickening and erosion and require some other heat source. Evidence of magmatic activity is abundant in the area with the Rathjen gneiss; a previously unidentified gabbronorite and leucogabbro and amphibolite dykes all being capable of supplying additional heat to the area through various stages of the metamorphic history.

1 INTRODUCTION

1.1 AIMS AND OBJECTIVES

The rocks in the Springton area of the Southern Adelaide Foldbelt (Figure 1) include metasediments of the Kanmantoo Group and a variety of syn and post tectonic intrusive rocks including the Rathjen gneiss. The specific aim of this work is to document the structural and metamorphic history of the Rathjen gneiss and the surrounding metasediments. This involves elucidating currently contentious issues concerning the origin and deformational history of the Rathjen gneiss. The metamorphic history of the area is documented using mineral assemblages from rocks of different ages. In the course of this work a number of previously undiscovered lithologies have been identified. These are described and correlated with other known rocks of the Kanmantoo sequence. These specific aims are all directed to building a more concise regional tectonic and metamorphic model for the Kanmantoo sequence in the vicinity of Springton.

1.2 GEOGRAPHICAL LOCATION AND SETTING

The area mapped in this thesis is just south of Springton, east of the Mount Lofty Ranges, South Australia. The areal extent is shown by Map A (Appendix 4). This encompasses the southern part of the Angaston topographic sheet (1:50,000) and the northern part of the Tepko sheet (1:50,000). With the exception of the Rathjen gneiss the quality of outcrop is generally poor, being scarce in many places, deeply weathered and extensively covered with lichen. The terrain is gently undulating with only a few peaks, such as Cookes Hill, standing above the surrounds.

1.3 PREVIOUS GEOLOGICAL INVESTIGATION

The Springton area has been previously mapped by Markham, 1951; Mills, 1964 and Mancktelow, 1979. The Rathjen gneiss has been investigated by Rattigan and Wegener, 1951; White, 1966 and Jenkins in press. The metamorphism of the area has been studied by Fleming and White, 1968 ; Allen, 1977 and Sandiford, Oliver, Mills and Allen, in press. General studies of the Kanmantoo in the Mount Lofty Ranges have been undertaken by Talbot, 1964; Offler, 1963; Mills, 1963, 1964, 1973; Kleeman and Skinner, 1959 and Marlow and Etheridge, 1977.

Figure 1 Locality map of the mapped area (C) showing position relative to Australia (A) and South Australia (B).

FIGURE 1

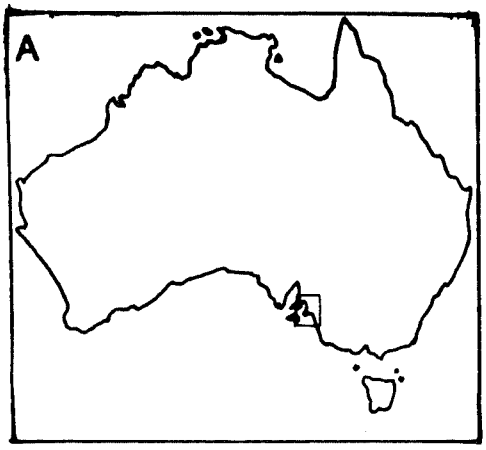
A

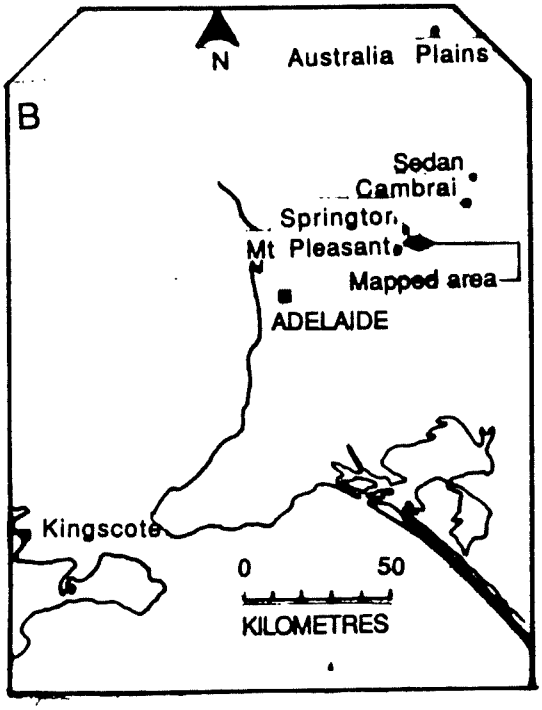
N
Australia Plains
B
Sedan
Cambrai
Springton
Mt Pleasant
Mapped area
ADELAIDE
Kingscote
0
50
KILOMETRES

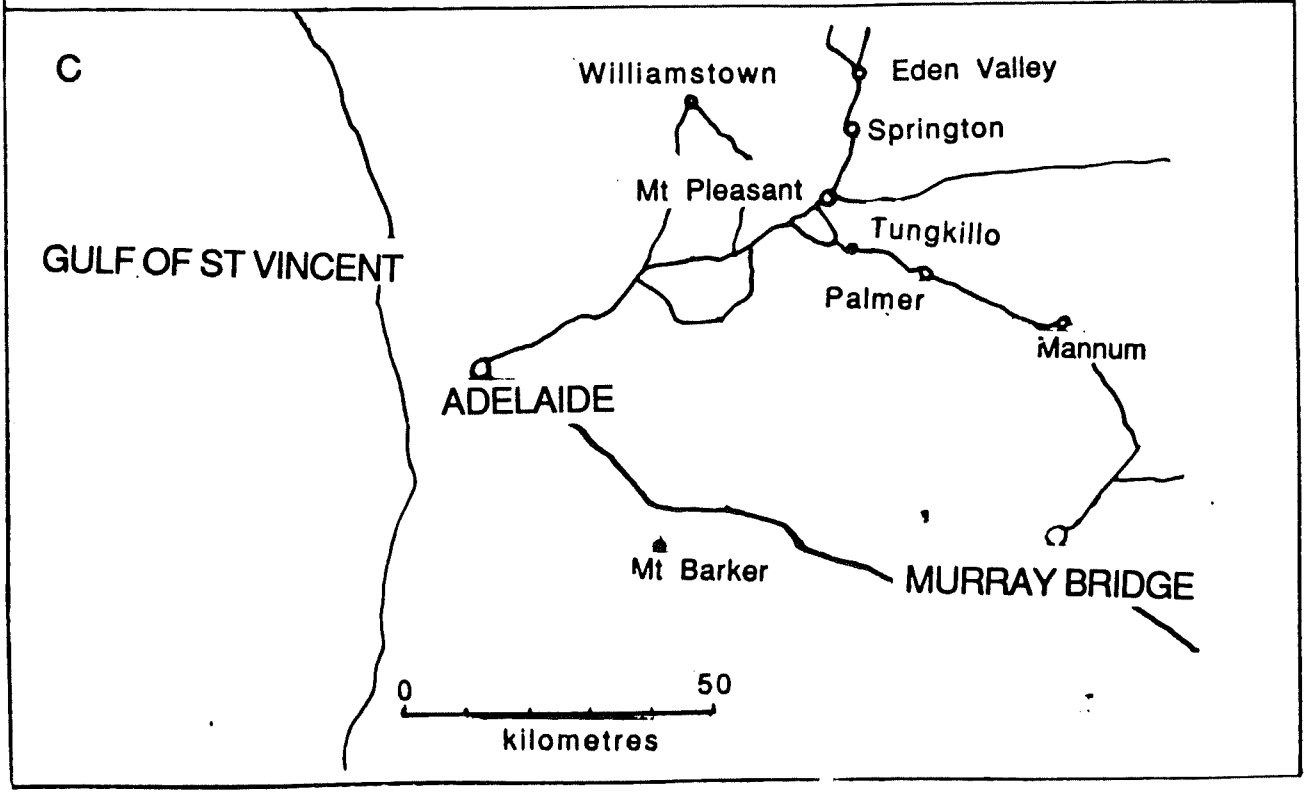
C
Williamstown
Eden Valley
Springton
Mt Pleasant
Tungkillo
Palmer
Mannum
GULF OF ST VINCENT
ADELAIDE
Mt Barker
MURRAY BRIDGE
0
50
kilometres

1.4 REGIONAL GEOLOGY

The Kanmantoo Group incorporates a rapidly deposited "flysch-like" sedimentary sequence (Milnes, 1982) that outcrops in the Southern Adelaide Fold belt over some 300 kilometres, from Kangaroo Island in the south to the Truro region in the north. Rocks of this sequence are essentially meta-sandstones, meta-siltstones and carbonates and were deposited during the lower to mid Cambrian (Sprigg & Campana, 1953). These metasediments are thought to be either in fault contact with the older Adelaidean sediments (Milnes, 1982) or in conformable contact with the Normanville Group.

Following accumulation, both the Kanmantoo and Adelaidean sediments in the Mount Lofty Ranges were metamorphosed and deformed during the Delamerian Orogeny. This orogeny commenced in the early-mid Cambrian and continued through to the lower Ordovician (Parkin, 1969; Daily et al., 1976) causing regional folding, faulting and sub-economic mineralization. The chronology of deformation has been discussed by Offler and Fleming (1968) and will be expanded upon in the following chapters.

Intrusion of granites, pegmatites and mafic dykes occurred throughout the Delamerian Orogeny. The timing of the intrusions in the Springton relative to metamorphic and deformation events will also be dealt with in the following chapters.

Generally acknowledged regional zones of metamorphism are displayed in Plate 1 (Preiss, 1987). They range from greenschist facies through to upper amphibolite facies. At the highest grades, partial melting is indicated by the formation of migmatites in the Springton and Palmer region. The association of the mineral isograds involving andalusite as opposed to kyanite has defined a "Buchan style" metamorphism (Sandiford et al., in press).

Plate 1 Map of:

(1) location of Delamerian granitoids after Flint and Parker,

(2) zones of metamorphism after Offler and Fleming, 1968

(3) zone of magnetic anomalies in Tapley Hill Formation after McKirdy et al., 1975.

Entire map after Preiss, 1987.

PLATE 1

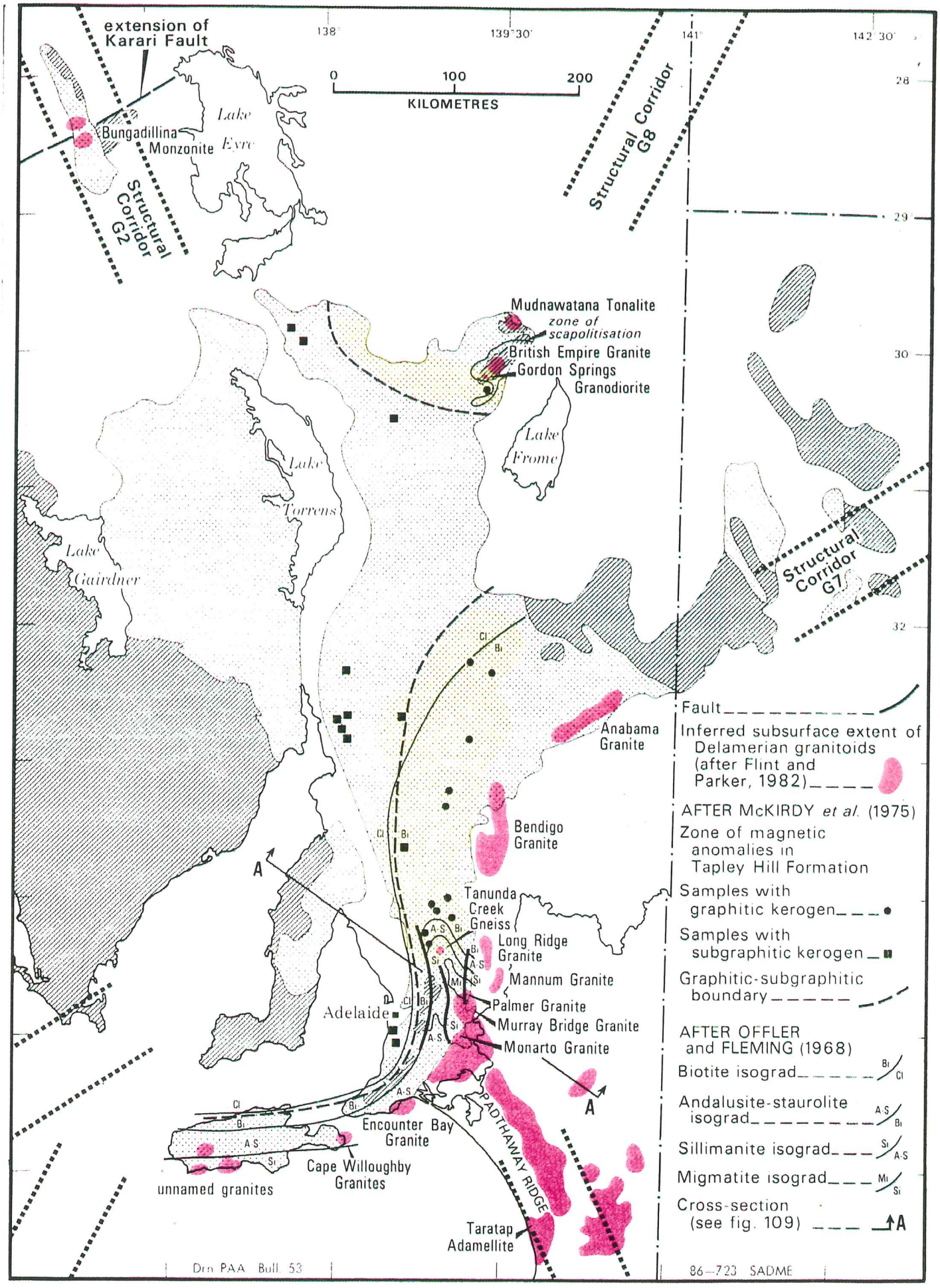

Fig. 108 Metamorphism and granitoid intrusions of the Delamerian fold belt.

2. LITHOLOGIES

2.1 INTRODUCTION

The mapped area occurs within the zone of highest grade of metamorphism in the Kanmantoo sequence, namely above the sillimanite isograd and within the migmatites zone. The major structural feature of the mapped area is a large, shallow SSE plunging syncline (Map A, Appendix 4). This syncline is cross cut by a series of right lateral transform faults. A number of dykes and sills have intruded the sequence, some prior to the formation of the syncline and others after its formation. The principal rock types identified within the mapped area are: the Rathjen gneiss; biotite migmatites, gneiss' and schists; talc rock; calcsilicate gneiss; albitized phyllite and epidote gneiss. Intrusive dykes and sills include an epidote aplite; a gabbronorite; an amphibolite and a leucogabbro. In this chapter these lithologies are described in order to provide a basis for a detailed discussion of the metamorphic and structural relationships of the Rathjen gneiss and the host metasediments.

2.2 THE RATHJEN GNEISS

The Rathjen gneiss outcrops in the core of the major syncline. It is a granitic, lineated and foliated gneiss, forming rounded boulders or tors as a result of exfoliation (Plate 2A and 2B). The principal minerals present include plagioclase (An_{25}), orthoclase, quartz, biotite and hornblende with occasional tourmaline, muscovite and magnetite. It is characterised by equilibrated metamorphic textures with polygonal grain boundaries. The lineation and foliation in the Rathjen gneiss are defined by the preferred dimensional orientation of both hornblende and biotite. Intrusive contacts with the biotite schist and gneiss suggest a plutonic origin for the Rathjen gneiss. The nature of the contact will be dealt with in subsequent chapters.The Rathjen gneiss includes mafic enclaves ranging from 2 to 10 centimetres in size, usually consisting of an aggregate of lineated biotite and hornblende with a finer quartzo-feldspathic matrix (Plate 2C).

2.3 THE BIOTITE RICH METASEDIMENTS

The biotite rich metasediments have been subdivided into three rock types on the basis of their fabrics; a biotite schist, a biotite gneiss and migmatite.

Plate 2A Outcrop form of the Rathjen gneiss.

2B Boulder of Rathjen gneiss.

2C Elongate xenolith within Rathjen gneiss.

2D Biotite sillimanite schist showing microfolding

2E Migmatite showing leucosome, melanosome and mesosome.

2F Intrusive contact of epidote gneiss with brecciated albitized phyllite.

PLATE 1

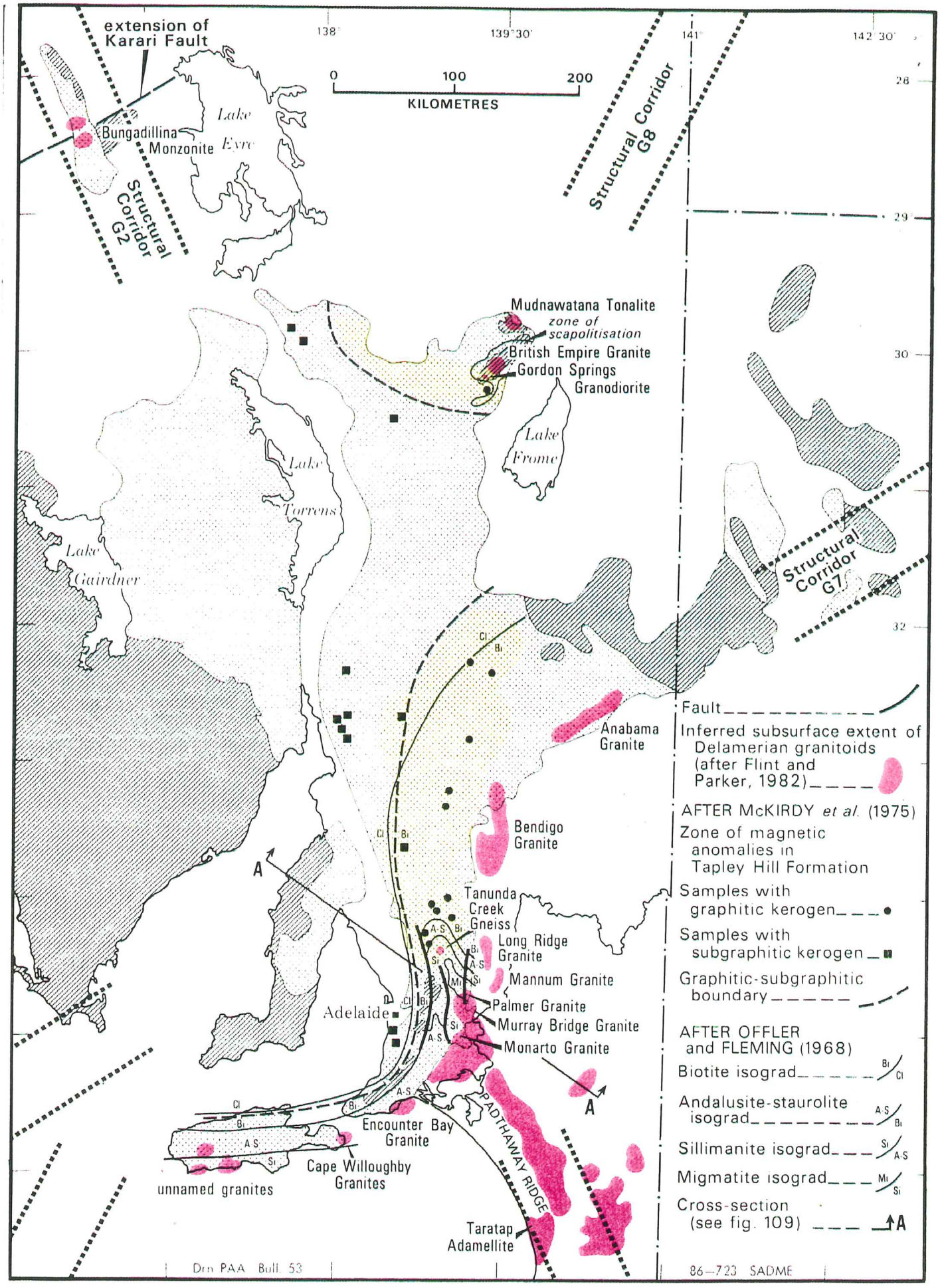

Fig. 108 Metamorphism and granitoid intrusions of the Delamerian fold belt.

PLATE 2

A

B

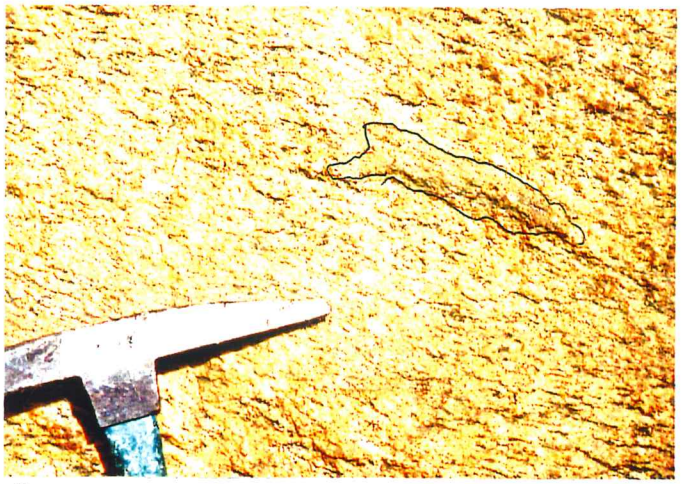

C

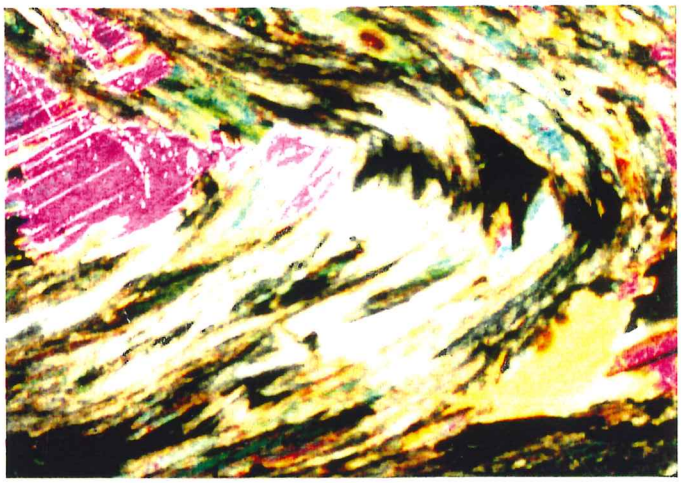

D

E

2.3.1 THE BIOTITE SCHIST

The biotite schist is a plagioclase (An_{12}), orthoclase, quartz , biotite and muscovite foliated metasediment with abundant sillimanite and rutile and minor ilmenite, magnetite, apatite, zircon and chlorite. The outcrop pattern of the biotite rich lithology resembles flaggy 'tombstones'. The biotite schist is of medium grain size (2 mm). Quartz grains in recrystallized, coarse felsic layers contain fluid inclusions indicating the presence of fluids during recrystallization. In thin section, all minerals except chlorite show low energy grain boundary configurations such as triple points indicating textural equilibration. The lower contact of the biotite schist with the calc silicate gneiss is parallel to compositional layering suggesting a conformable sedimentary contact. However sedimentary features are obliterated by the high degree of deformation and metamorphism in this area, and this apparent conformity may be due to subsequent intense deformation (Plate 2D). (See later discussion).

2.2.2 BIOTITE GNEISS

The biotite gneiss is a plagioclase (An_{10}), orthoclase, quartz, biotite metasediment that is obviously genetically related to the biotite schist, but of a more felsic character. It forms more rounded outcrops and is coarser grained than the schist. It is particularly coarse grained to the west of the syncline .

2.2.3 MIGMATITES

Adjacent to the Rathjen gneiss, the biotite schist develops a characteristic migmatitic fabric defined by the development of quartz and plagioclase (An_{10-12}) leucosomes. Otherwise the mineralogy is identical to the biotite schist. Individual leucosomes define a stromatic or layered fabric (Plate2E). As the biotite schist and gneiss show a gradational contact with the migmatites approaching the Rathjen gneiss, it is assumed that the migmatites represent the partially melted equivalent of these lithologies. The migmatites will be discussed in greater detail in Chapter 6.

2.4 TALC ROCK

The talc rock occurs as large lenses (approximately 2m in length) in the biotite gneiss. The mineral assemblage is quartz, plagioclase (An_{10}), orthoclase and talc with minor biotite,

ilmenite and rutile. The outcrop form is distinctly nodular. Petrographically quartz forms recrystallized mosaics around plagioclase laths. Orthoclase forms large poikiloblasts and shows replacement by talc. Talc forms green radiating masses.

2.5 CALCSILICATE GNEISS

The calcsilicate gneiss is a lineated scapolite, diopside, plagioclase (An5), actinolite bearing rock. Recrystallized quartz grains surround the scapolite porphyroblasts. Apatite and sphene are abundant whilst accessories include epidote and zircon. It typically outcrops as rubble with only small angular blocks protruding at the surface. The amphiboles define a mineral elongation lineation plunging gently to the south. There is a distinct decrease in grainsize from north to south, approaching a mylonitic fabric in the south of the mapped area near Cookes Hill Road. The contact with the albitized phyllite (described below) appears conformable, suggesting a sedimentary sequence whilst it has been intruded by the epidote gneiss (described below).

2.6 ALBITIZED PHYLLITE

The quartzo-albitic (An5) phyllite exhibits a characteristic sugary texture with a distinctly flaggy outcrop pattern. It has minor biotite, actinolite and rutile. The ferromagnesian minerals define a compositional lineation. Petrographically, albite is either poikiloblastic or else in needle form with a preferred orientation and orthoclase has a decussate form. It is cross cut by the epidote gneiss and is stratigraphically conformable with the calcsilicate gneiss (Plate 2F).

2.7 EPIDOTE GNEISS

The epidote gneiss is a medium to coarse grained meta-intrusive which shows preferential alignment of minerals and gneissic banding. It shows cross cutting relationships with the metasediments. The epidote gneiss consists of porphyroblastic quartz, orthoclase, oligioclase and epidote with minor biotite, muscovite and ilmenite. Texturally equilibrated grain boundaries indicate metamorphism as does the preferential layering of felsic and mafic minerals.

2.8 EPIDOTE APLITE

The epidote aplite is a fine to medium grained epidote bearing felsic meta-intrusive which shows no preferential alignment of minerals. It outcrops only to the east of the syncline. Quartz, orthoclase and plagioclase (An_{25-27}) form both porphyroblasts and smaller subhedral crystals. Feldspar zoning indicates relict igneous textures. The minerals exhibit low energy, polygonal grain boundaries indicative of metamorphic equilibration. Epidote forms small subhedral grains. Sphene, biotite and muscovite form accessory minerals.

2.9 GABBRONORITE

A gabbroic intrusive outcrops in the south east corner of the mapped area. It is a pyroxene amphibole gabbronorite that progressively changes in texture from south to north. The southern most end of its outcrop displays a random relict igneous fabric of hornblende, plagioclase (An_{75}) laths and exsolved pyroxene in a groundmass of predominantly anhedral actinolite. Quartz grains form a mosaic of secondary grains around the plagioclase laths. Plagioclase shows distinct zones, the cores being substantially more calcic than the rims (An_{75} cores, An_{45} rims). The laths are often subhedral showing symplectite reaction textures with the amphibole groundmass (Plate3A, B and C). In contrast, the northern end of this outcrop has a porphyritic texture and is characterized by phenocrysts of plagioclase in a fine grained groundmass of subhedral actinolite and pyroxene. Plagioclase is poikiloblastic and contains hornblende inclusions as does the coarser grained equivalent. Relict igneous plagioclases (An_{77}) are mantled by recrystallized rims of (An_{45}). These recrystallized fabrics show equilibrated triple point contacts (Plate 3D). The other remarkable feature in this part of the intrusion is that the anorthite rich cores are all extensively fractured (Plate 3F). Pyroxene is uralitized and has a composition ranging from diopside to augite. The gabbronorite shows little deformation compared with the lineated, foliated amphibolite dyke 200 metres to the east although the textural relationships clearly suggest that this gabbronorite has suffered metamorphism.

2.10 LEUCOGABBRO

The leucogabbro is an undeformed holocrystalline igneous rock with random and extensive development of amphiboles (Plate 3E). The felsic minerals are plagioclase (An_5) and

Plate 3A Gabbronorite showing symplectite reaction texture between actinolite and calcic plagioclase.

3B Scanning electron microprobe compositional image of a similar texture in the gabbronorite.

3C Increased magnification of 3A, texture bottom left.

3D Re-equilibrated boundaries of plagioclase (An77) and (An45) in gabbronorite. Compositional image from electron microprobe.

3E Leucogabbro with randomly orientated amphibole laths.

3F Electron microprobe compositional image of plagioclases of the gabbronorite. Shows extensive fracturing of the more calcic component.

3G Weathered amphibolite dyke showing cross cutting relations.

PLATE 3

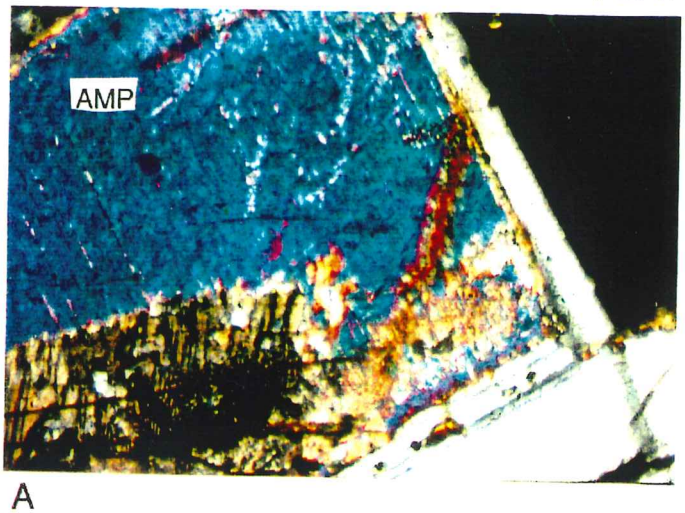

A

B

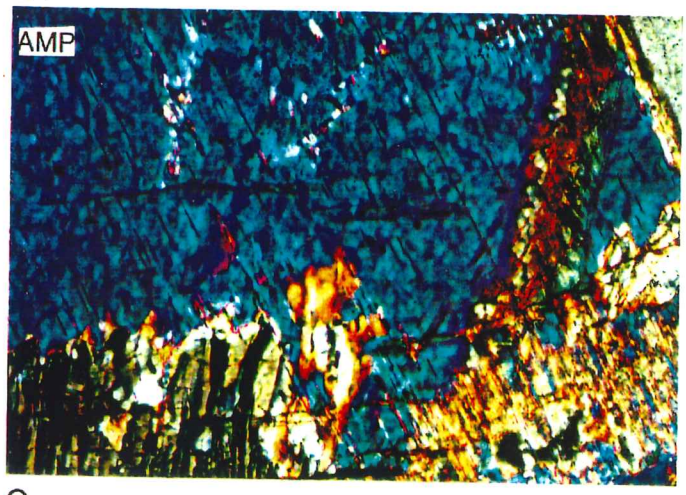

C

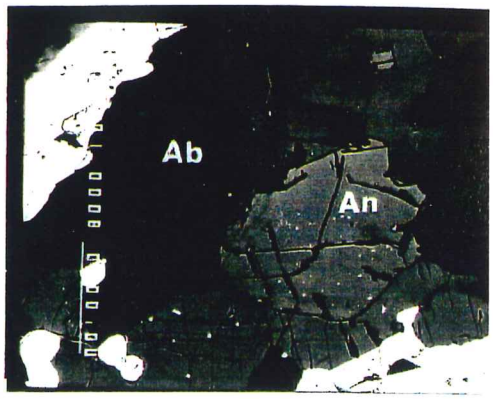

D

E

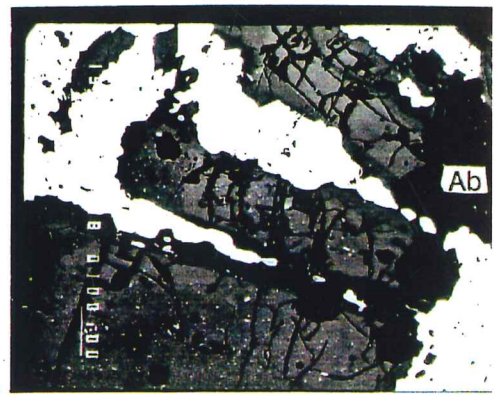

F

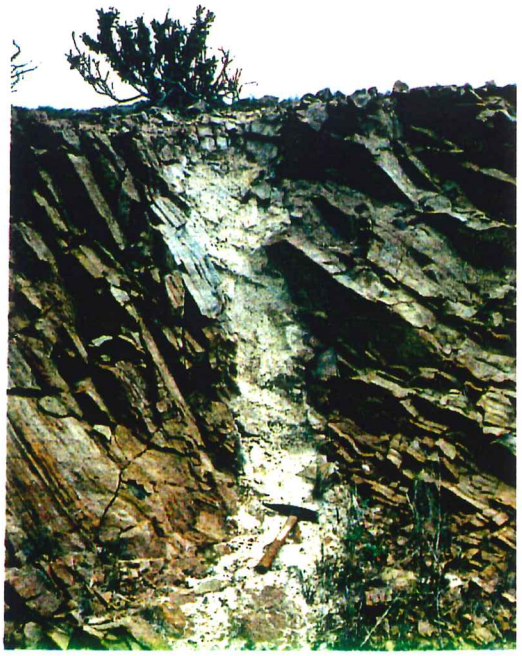

G

microcline. Accessory minerals include rutile, apatite and zircon. The grain boundary relationships show the felsic minerals in equilibrium. The amphibole is compositionally unusual, being a calcic rich actinolite (See Appendix 2 for probe results)

2.11 AMPHIBOLITES

Amphibolite dykes and sills have intruded various lithologies in the Kanmantoo and in this area they are found within the epidote gneiss and within the albitized metasediment. They outcrop as strongly defined ridges and are usually about 100m in length. The dykes (Plate 3G) are characterized by lineated hornblende, plagioclase (An_{40}), orthoclase and quartz. Magnetite, ferro-ilmenite and biotite are accessory minerals. The felsic and mafic components show a metamorphic layering. Relict igneous textures include zoned plagioclase.

3. STRUCTURAL HISTORY

3.1 INTRODUCTION

The structural history of the Springton region has been somewhat neglected since the definitive paper by Offler and Fleming in 1968. This chapter will describe the local structural history from field evidence. The Delamerian Orogeny has long been recognized as a period of intense deformation and metamorphism which commenced in the early Cambrian and continued through to the lower Ordovician in Australia (Thomson, 1969; Mancktelow, 1979). In Australia its effects were most pronounced in the Adelaide geosyncline and the Kanmantoo trough, though it was temporally associated with a much more widespread fold belt which included the Ross Orogen in Antarctica. The prevailing view is that Delamerian deformation produced east west shortening in the Kanmantoo associated with three phases of folding (Offler & Fleming, 1968). Importantly this chapter will provide evidence for previously unrecognized N-S tectonic transport early in the deformation history of the Kanmantoo.

3.2 DEFORMATION AT SPRINGTON

In accordance with other work (e.g. Offler and Fleming, 1968) three phases of folding are recognized in the Springton region. The first phase of folding, F_1, is recumbent and isoclinal. Fold limbs are subhorizontal and axial planes trend E-W as a consequence of subsequent upright folding about N-S trending axes (Plate 4A). F_2 is represented by upright, open folds and the axial planar schistosity, S_2, is the dominant foliation in many of the metasediments. F_2 is expressed in the Springton area as the major syncline gently plunging SSE at approximately 10 degrees. F_2 is particularly well developed in the less competent lithologies which show abundant parasitically folded F_2 (Plate 4B, C and D). The third phase of folding, F_3, is represented by a series of open upright to slightly reclined mesoscopic folds. The F_3 folds refold both F_1 and F_2 and produce complex interference patterns of dome and basin form (Offler and Fleming, 1968). The F3 folds have axial planes trending NW with SE-trending axes plunging 25 ^{o} SE.

Brittle faulting has also occurred, displacing axes of all three fold generations. From mapping these are identified as a series of right lateral transform faults. These faults are

Plate 4A Shows F1 isoclinal recumbent folding of leucosomes in migmatites.

4B Shows parasitic F2 upright open folding in the biotite gneiss.

4C A close up of 4B

4D Shows parasitic F2 upright folding in the albitized phyllite.

4E S1 foliation of the Rathjen gneiss.

4F Stretching lineation of the Rathjen gneiss.

PLATE 4

A

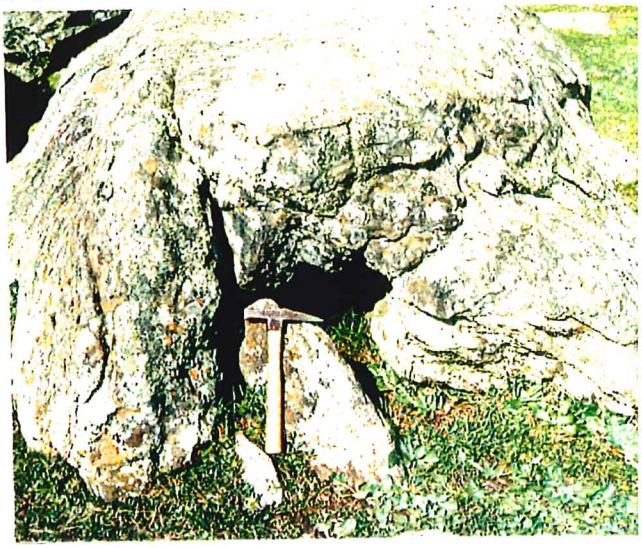

B

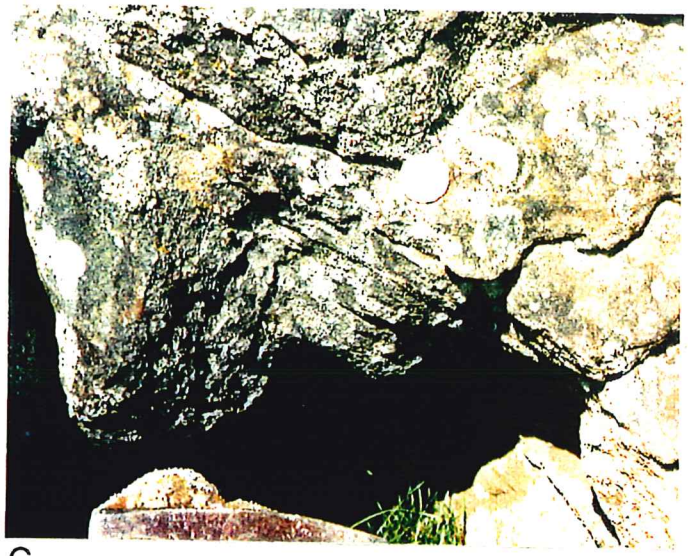

C

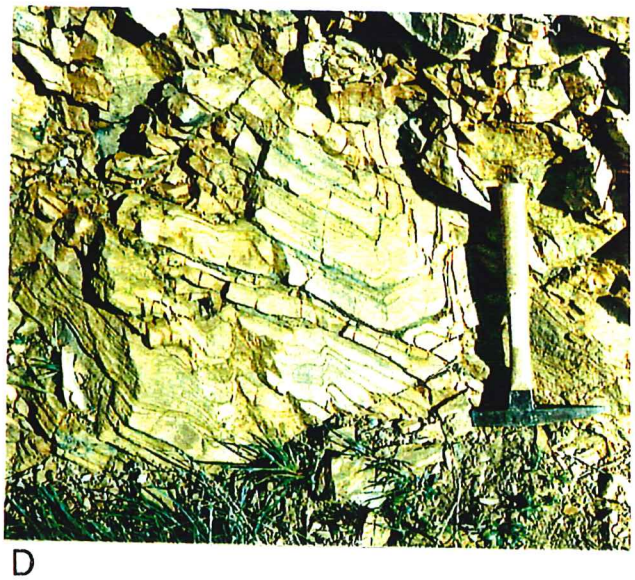

D

E

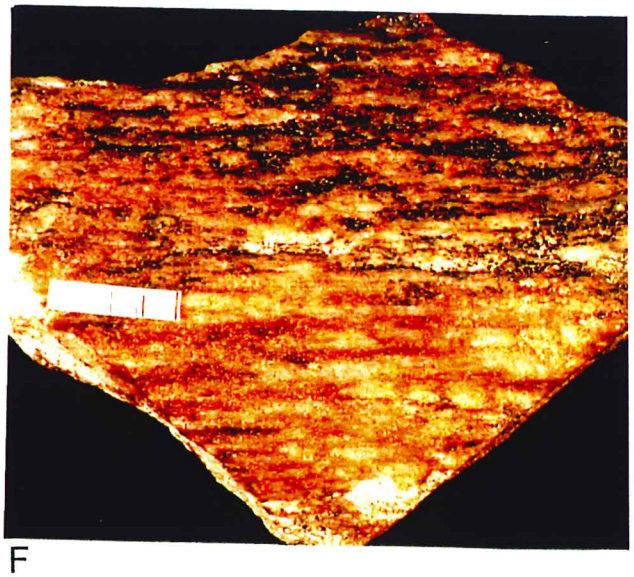

F

associated with slickenside structures in the biotite schist, fault breccia in the albitized phyllite and quartz veins up to 10 metres long within fault zones. Although it is difficult to establish in the field, these faults seem to have affected the Rathjen gneiss displacing the F_2 fold axes. Geophysical data in the form of radiometrics support this displacement (S.Rajagopalan, pers. com. 1988).

3.4 THE STRETCHING LINEATION

A previously uninterpreted stretching lineation is preserved in the more competent lithologies of the mapped area and is particularly well developed in the Rathjen gneiss. Because of the fundemental importance of stretching lineations in the the understanding of orogenic belts (e.g. Shackleton and Ries, 1984), this stretching lineation will be described at some length.

In the Rathjen gneiss the stretching lineation is defined by the elongation of biotite, hornblende and tourmaline. The foliation and lineation of the Rathjen gneiss are displayed in Figures 4E and 4F respectively. The general orientation of this lineation is N-S (Figure 2). In the south east of the mapped area there is an outcrop of the calcsilicate gneiss that has been extensively mylonitized with elongate quartz flaser textures. The orientation of this lineation is also N-S Both the amphibolite dyke and the biotite gneiss to the south of the area show a similar stretching lineation. The elongation of biotite and hornblende are evident in both lithologies. The elongation of felsic minerals in the biotite gneiss also reflects this stretching lineation. The orientations of these lineations are not clearly N-S, but seem to vary along strike from NNW to N-S..

Since this N-trending lineation has been folded by F_2 it is believed to predate F_2. It is of similar orientation to the F_1 mesoscopic isoclinal folds observed in the biotite schist and migmatite, and therefore is interpreted as being coeval with F_1. Importantly only in the competent lithologies such as the Rathjen gneiss is this original N-S orientation preserved.

A strong N-S lineation is somewhat unexpected considering the general belief that the Foldbelt was deformed by east west shortening (Offler and Fleming, 1968; Jenkins, in press; Preiss, 1987). The N-S orientation of this stretching lineation in the competent lithologies

Figure 2 Map of the orientation of the stretching lineation within the Rathjen gneiss. Faults and their displacement are only inferred from geophysical data. Fold axes define F2, the shallowness of their plunge effecting the recognizable displacement.

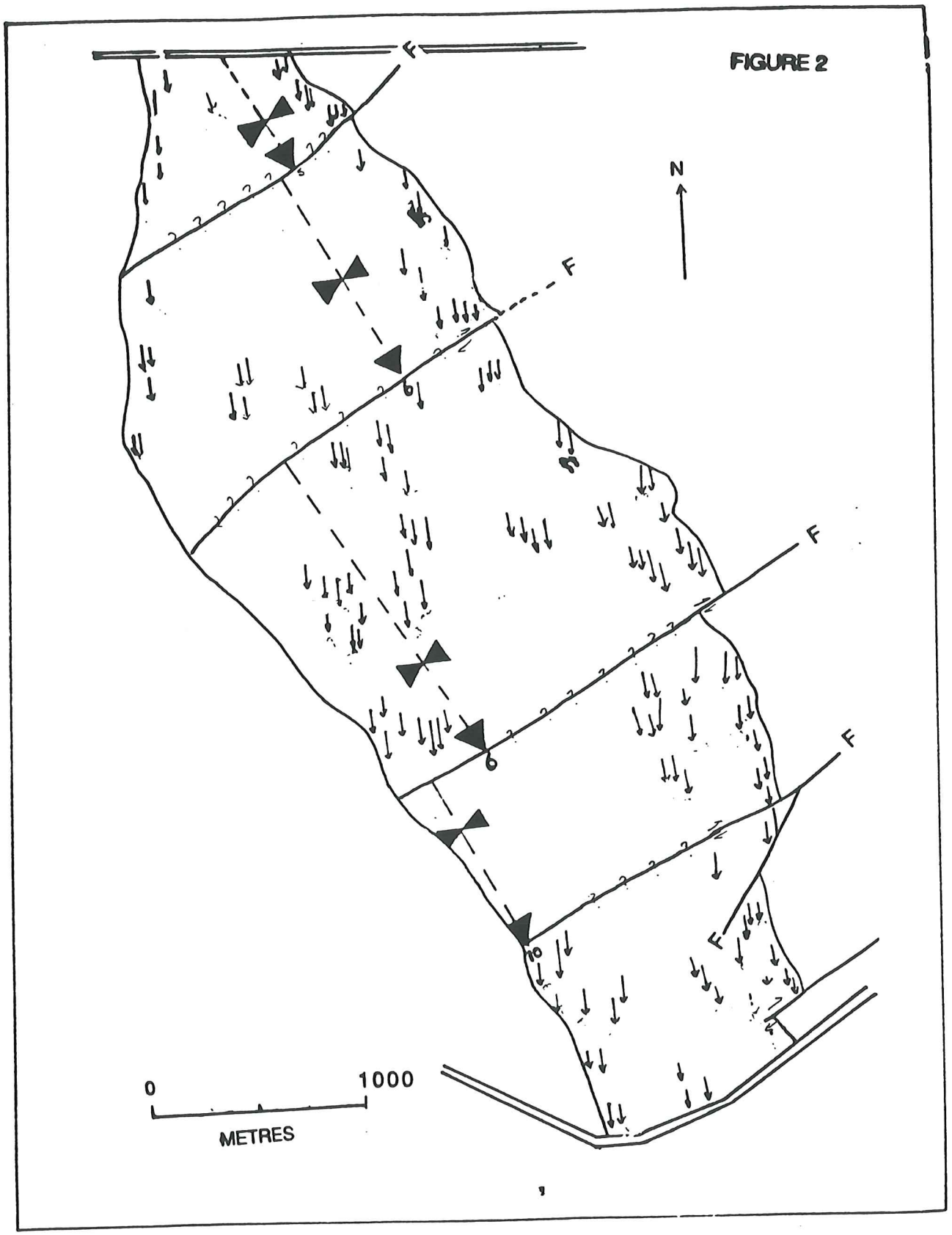
FIGURE 2
N
F
F
F
F
0
1000
METRES

implies that early in its history, the Foldbelt must have been tectonically transported in this direction (Shackleton and Ries,1984). It is possible that this stretching lineation in the Rathjen gneiss and the calcsilicate be correlated with the N-S orientated Marne River mylonites although as yet the significance of these mylonites is unknown.

4. ORIGIN OF THE RATHJEN GNEISS

4.1 INTRODUCTION

Granites have long been considered fundamental components of crustal tectonics and orogenic belts. It has been suggested that the type of granite is diagnostic of the tectonic setting in which it formed (Pearce, 1983; Pitcher, 1982). This is because the different compositions of granite are intrinsically related to the source rocks and also the environmental (pressure and temperature) characteristics of each particular tectonic setting (Turner, 1986). I have shown from structural evidence that the Rathjen gneiss is unique in preserving evidence of a previously unrecognized deformation in the Kanmantoo, but even now there is no clear consensus as to whether it represents an intrusive or volcanic rock. The types of models proposed are two-fold; (1) that it is a metamorphosed intrusive granite (Rattigan and Wegener, 1951) and (2) that it is a metamorphosed acid volcanic tuff (White, 1966). In this section new evidence will be used to refute the arguments of White (1966) and others (e.g. Fleming and White, 1968) concerning its genetic character. To be fair, each of the main points used by White (1966) to argue for a volcanic origin will be discussed.

4.2 EVIDENCE OF GENESIS

White (1966) maintains that although its coarse grained habit and the lack of the zoned plagioclases suggest an intrusive origin, the lack of xenoliths, its geochemistry, the overall shape of the body and the field relations suggest that its is an acid volcanic flow that has been metamorphosed.

4.2.1 FIELD CRITERIA

The coarse grained nature of the Rathjen gneiss is consistent, but not necessarily indicative of an intrusive origin. If it were originally an acid volcanic rock this would imply the metamorphism had resulted in considerable grain coarsening. In adjacent metapsammites of essentially the same predominant mineralogies, i.e. quartz and feldspar, there is little evidence for such grain coarsening, whilst it is evident in much more K-rich rock types such as the pelites. These observations suggest that the fabrics present in the gneiss are unlikely to

result from an initially fine grained volcanic rock but is more consistent with an initially coarse grained intrusive rock.

White (1966) argues that an absence of xenoliths in the Rathjen gneiss is inconsistent with an intrusive origin, an argument that is essentially contentious since it is possible for an intrusive rock not to have xenoliths. Moreover, it is possible for a volcanic to entrap foreign objects during transportation and emplacement. Contrary to White (1966), I have observed numerous examples of xenoliths in the Rathjen gneiss (Plate 2C). These range from 5 to 10 cm in length. Compositionally they are mafic igneous rocks, being composed essentially of hornblende and plagioclase which is consistent with the genetic model proposed below. Their elongate shape is consistent with having suffered considerable stretching during the formation of the mineral elongation lineation.

The argument used by White (1966) that the shape of the body is inconsistent with a granite pluton can be addressed in various forms. One is that we are looking at a lithology that has been intensely deformed, thus its present shape may show little resemblance to its initial shape. With the present poor constraints on finite strain it is equally possible that its prestrained form was that of a laccolith or that it was an equidimensional blob. The main thrust of this argument against shape being indicative of a genetic environment is that the present shape of the Rathjen gneiss reflects its deformational history; that is, a number of generations of stretchings, folding and faulting define the current shape of the body, not its genetic character. Thus the present shape of the Rathjen gneiss is a product of its tectonic history. To ascribe a genetic environment from its present shape fails a priori to recognize this fact.

The final field argument and perhaps the most critical of White's (1966) is that the contacts between the Rathjen gneiss and the metasediments do not show intrusive relationships. He maintains that small tuff horizons are interbedded with the biotite schist and that the Rathjen gneiss is a larger scale expression of this relationship. My observations around and along the contact of the Rathjen gneiss and the biotite schist demonstrate two diagnostic features. Firstly, as the biotite schist approaches the gneiss there is a noticeable

increase in the melt percentage. Secondly, there are portions of Rathjen gneiss within the biotite schist, which show clear intrusive relationships (Plate 5). I suggest that the thin layers that seem "interbedded" with the metasediments represent apophyses of the intrusion which have been rotated into parallelism with the contact during the subsequent intense deformation.

4.2.2 GEOCHEMICAL CRITERIA

White (1966) further maintained that the compositions of felsic minerals do not plot as the minimum melt on a granite normative diagram (Fig 3A and B) and that the minor element analysis and rare earth ratios are different to those of the neighbouring Palmer Granite. In light of the findings of Foden et al. (in press) it is not surprising that the geochemistry of these two rocks are different since the Palmer granite is manifestly post-tectonic. Table 1 shows whole rock analyses of Rathjen gneiss, an average syn Delamerian granite and an average post Delamerian granite from Foden et al. (in press). Figure 4 is a spidergram of the incompatible trace element data in table 2 normalized to continental crust. Foden et al. (in press) have shown that there is a marked distinction between the chemistry of syn and post Delamerian granites, a trend clear in Figure 4. It can be seen from this diagram that the Rathjen gneiss is comparable with the syn Delamerian granites in terms of the shape of the plot and the general trace element content whilst the post Delamerian granites are markedly different.

I-Type granites are characterised by certain geochemical parametres. The most diagnostic of these are ; (1) they are non peraluminous, i.e. mol $Al_2O_3/(Na_2O + CaO + K_2O)$ is less than 1.1; (2) the Na_2O percentage is greater than 3.2; and (3) the rocks are diopside normative (Chappell and White, 1974). Geochemical results tabulated in Table 1 indicate that the Rathjen gneiss is not peraluminous. The Na_2O percentage of the analysed Rathjen gneiss has a value greater than 3.2 and it is also diopside normative confirming that it indeed has I-Type granite geochemistry. Such a chemistry would not result from the anatectic melting of the metasediments, which would produce S-Type granites as proposed by Rattigan and Wegener (1951). Other evidence that it is not S-Type is the composition of biotite in the gneiss and the migmatites. The Al and Mg content of Rathjen gneiss and migmatite biotites are shown as Figure 5. The Rathjen gneiss compositions are comparable with the synDelamerian granites and very dissimilar to the metasediments, migmatites and post Delamerian granites. Clearly the

Plate 5A Rathjen gneiss cross cutting biotite schist as well as forming the "interbedded layers" described by White (1966).

5B Intrusive relationship

5C Intrusive relationship

5D Intrusive relationship

5E Rathjen gneiss discordance with biotite gneiss.

5F Close up of 5E

PLATE 5

A

B

C

D

E

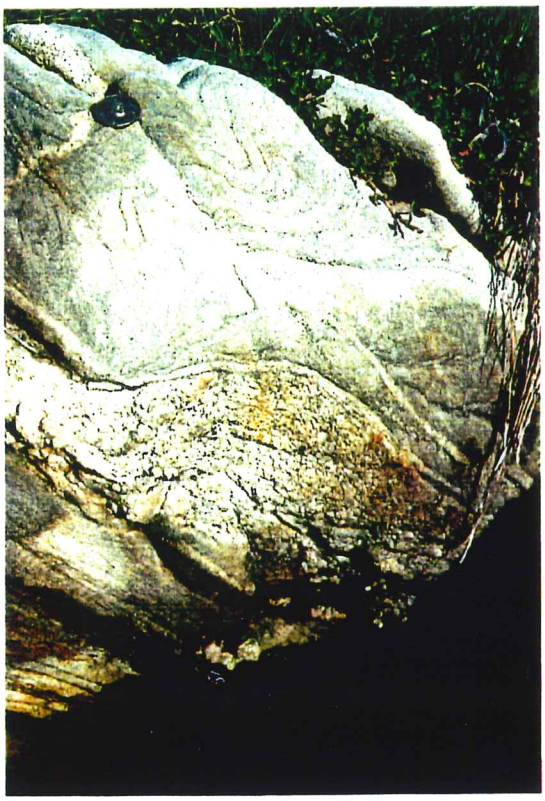

F

Rathjen gneiss is not an anatectic melt or an S-Type granite. This does not in itself preclude the Rathjen gneiss from being a meta-volcanic but does show that the geochemical argument is to a certain extent irrelevant as the ambiguity of the data sets lends itself to either an intrusive or extrusive interpretation.

4.2.3 CONCLUSIONS

The Rathjen gneiss is not a metamorphosed volcanic tuff as suggested by White (1966) as all the arguments used are either dated, ambiguous or simply wrong. Its field relations indicate it is of intrusive origin and that its genetic character was akin to an I-type granite, similar to the other syntectonic granites in the region (Foden et al., in press).

Figure 3A Ternary quartz, albite, orthoclase diagram of normative Rathjen gneiss, Average syn Delamerian granite and average post Delamerian granite.

3B Ternary anorthite, albite, orthoclase diagram of normative Rathjen gneiss, Average syn Delamerian granite and average post Delamerian granite.

FIGURE 3

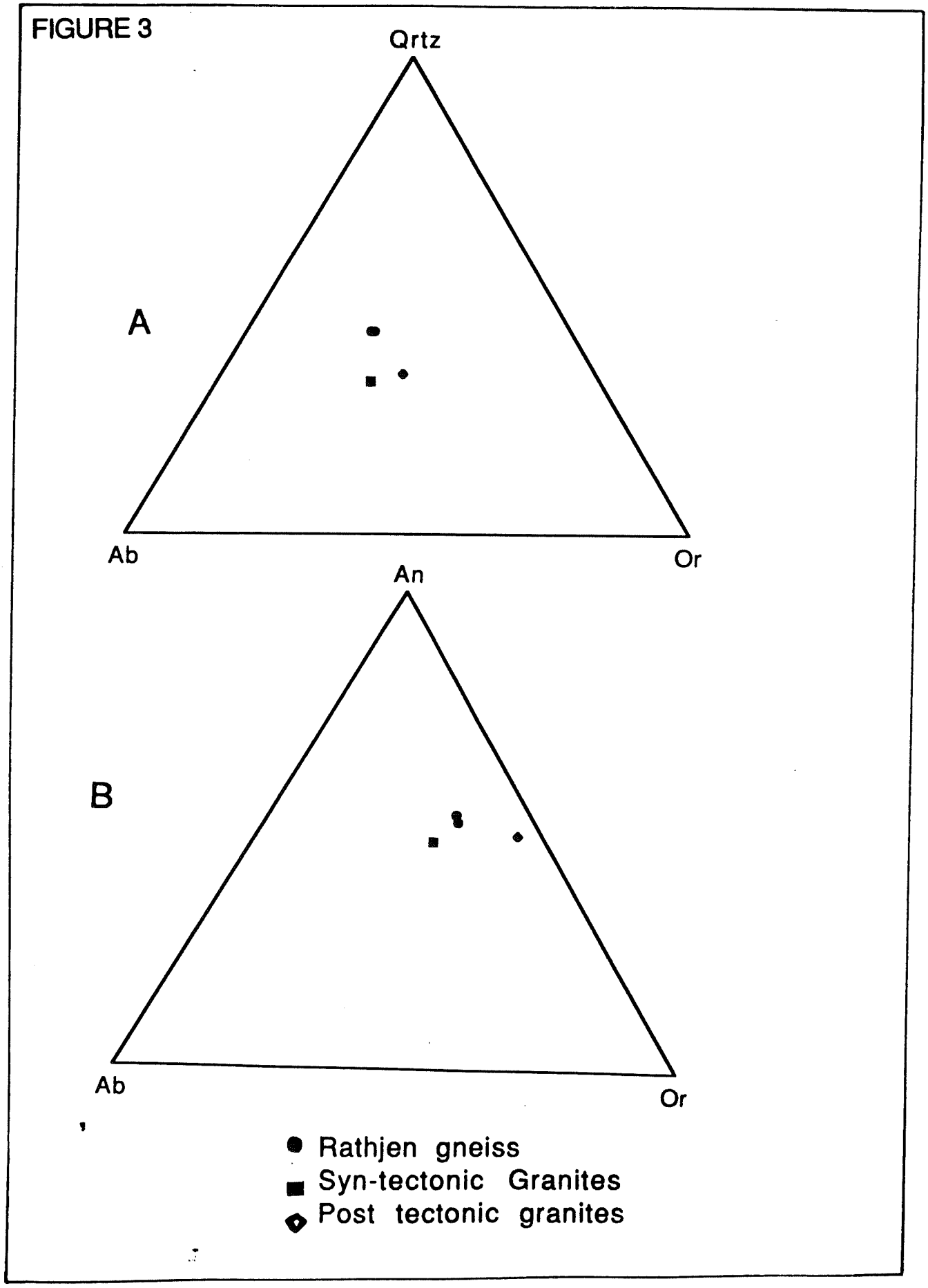
Qrtz
A
Ab
Or
An
B
Ab
Or
Rathjen gneiss
Syn-tectonic Granites
Post tectonic granites

Table 1 Whole rock and trace element analyses of the Rathjen gneiss (898-309); an average syn Delamerian granite and an average post Delamerian granite. Average syn and post Delamerian granite calculated from values given in Foden et al., in press.

Figure 4 Spidergram of incompatible trace elements of the Rathjen gneiss (898-309), average syn Delamerian granites and average post Delamerian granites. Spidergram is normalized to continental crust.

TABLE 1

	A	B	C	D
1	elements	898-309	av syn Dela	av post Dela
2	SiO2	73.97	69.17	75.15
3	Al2O3	12.45	15.23	12.84
4	Fe2O3	2.81	3.6	2.09
5	FeO	0	0	0
6	MnO	0.03	0.06	0.04
7	MgO	0.81	1.39	0.21
8	CaO	1.66	2.85	0.75
9	Na2O	3.55	3.75	3.78
10	K2O	3.17	3.62	5.11
11	TiO2	0.44	0.51	0.2
12	P2O3	0.1	0.15	0.03
13	SO3	0.02	0	0
14	LOSS	0.25	0	0
15	TOTAL	99.26	0	0

	A	B	C	D
1		898/309	av syn Dela	av post Dela
2	Sr ppm	115	345	52
3	Rb ppm	123	134	238
4	Y ppm	41	25	66
5	Zr ppm	260	65	232
6	Nb ppm	12.8	16	32
7	Ba ppm	697	827	270
8	Sc ppm	8.7	9	4
9	Ni ppm	7	18	4
10	V ppm	40	87	8
11	Cr ppm	17	25	1
12	Ga ppm	16	20	21
13	Ce ppm	102	65	123
14	Nd ppm	42	26	57
15	La ppm	48	32	73

FIGURE 4

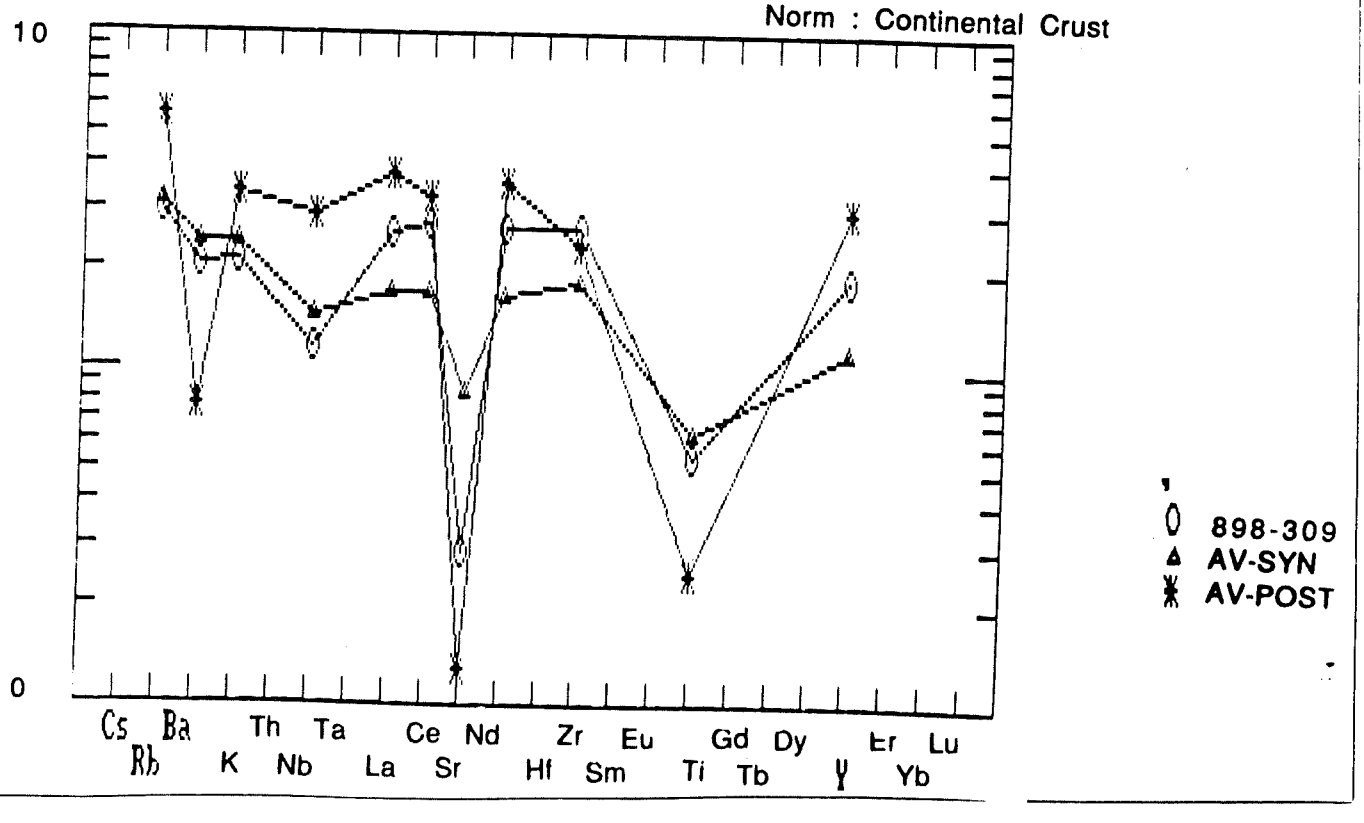

Figure 5 Comparisons of Al2O3 vs. MgO content of biotites from the Rathjen gneiss, syn Delamerian granites, post Delamerian granites, migmatites, metasediments and gabbros in the Kanmantoo Group.

FIGURE 5

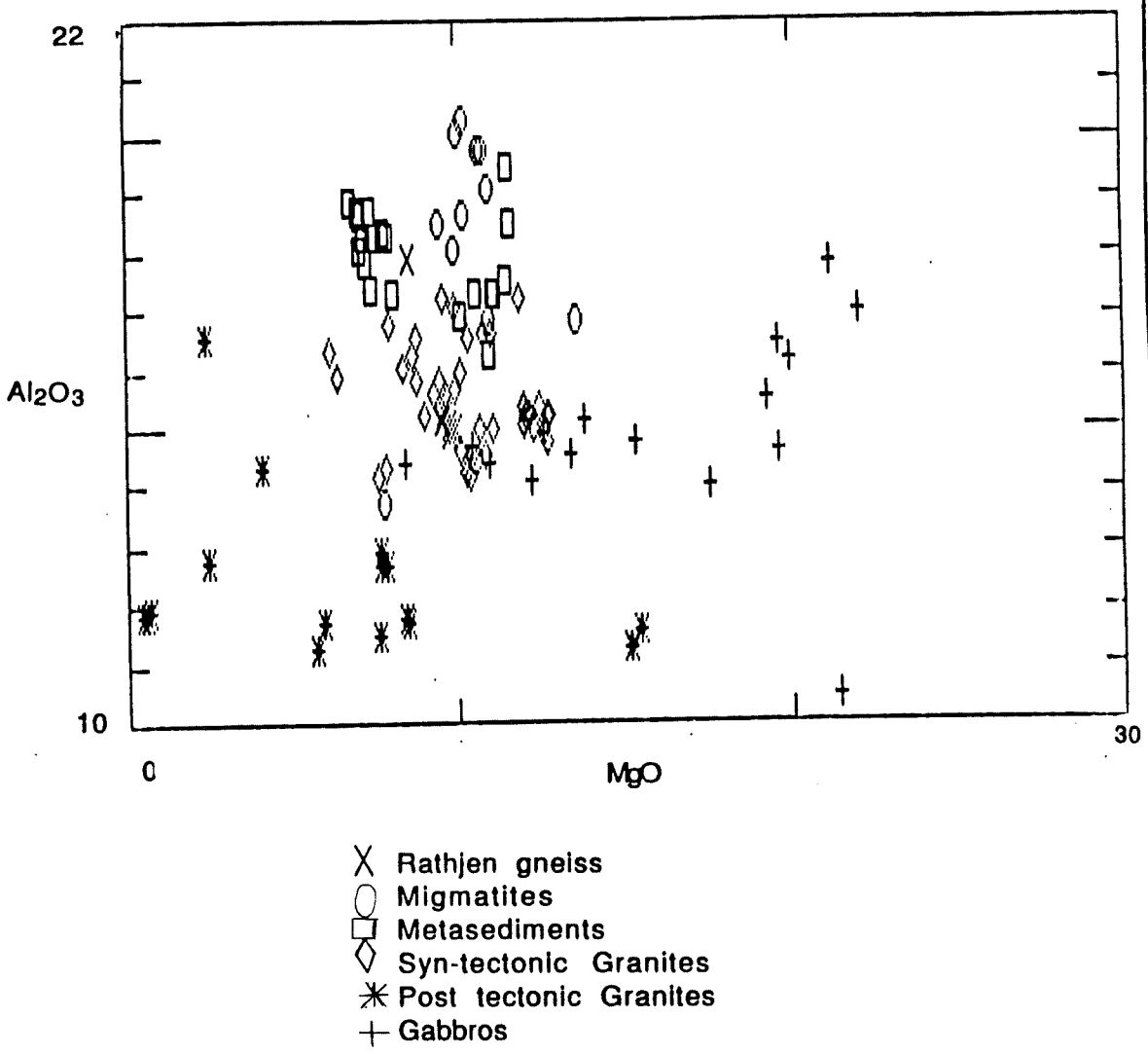
22
10
Al_2O_3
0
MgO
30
Rathjen gneiss
Migmatites
Metasediments
Syn-tectonic Granites
Post tectonic Granites
Gabbros

5. GEOCHEMISTRY AND PETROLOGY OF GABBROS

5.1 INTRODUCTION

During mapping, two previously unrecognized gabbroic outcrops were discovered. These are a gabbronorite and a leucogabbro, the petrographic descriptions of the rock types being in chapter two. These by in large preserve igneous textures and therefore are of great interest as they provide indications of thermal perturbations and the path of magmatic evolution in the Kanmantoo Group following Delamerian deformation.

5.2 GABBRONORITE

A gabbronorite outcrops in the southern part of the area, between the Rathjen gneiss and biotite gneiss contact. This area preserves a remarkable range of igneous rocks suggesting repeated exploitation by invading magmas. In addition to the Rathjen gneiss and the gabbronorite described, the region includes an amphibolite sill and possible Mesozoic dolerites found immediately to the south of the mapped area (J.Foden and M.Sandiford, pers.comm.). The amphibolite sill has been deformed and contains the dominant N-S stretching lineation, whilst the gabbronorite and the Mesozoic dolerite are undeformed. In hand specimen and thin section, this rock is similar to Black Hill Norite. Black Hill Norite is an igneous complex of mafic to ultramafic rocks, the main outcrop occurring at Black Hill on the Murray Plains. Black Hill Norite has been dated by a Rb-Sr Biotite whole rock isochron and given an age of 487 $\pm$ 5 Ma. (Milnes et al., 1977). The outcrop of the gabbronorite is generally poor with the southern outcrop generally coarse and more equant and the northern outcrop fine grained with porphyroblasts of quartz and feldspar which is suggestive of a chilled margin.

Geochemical analysis of the two phases are given in Table 2. Also included in this table is an average geochemical analysis of Black Hill Norite (BHN 2) that is used as a standard in the Department of Geology at Adelaide University.

In terms of major element geochemistry comparison, the gabbronorite, show significant variation in the Al_2O_3, MgO and SiO_2 values from the BHN 2. It contains more Al_2O_3 and less SiO_2. However the Black Hill complex shows a wide range of chemical compositions as a result of combined fractionation and assimilation affects (S.Turner,

pers.comm.), with its range inclusive of these Springton gabbronorites. The gabbronorites are then broadly compatible with the range of samples from the Black Hill complex.

Figures 6 and 7 are spidergrams of incompatible trace element plots. These spidergrams provide a convenient graphical means of comparing trace element chemistry's which are less sensitive to fractionation. Figure 6 shows spidergrams of the mapped gabbronorites. Figure 7 is a spidergram of a range of gabbros from Black Hill. The concept behind these patterns is that apart from Sr, variation in the degree of partial crystallization will change the level of the pattern but not the shape. Therefore an average tholeiitic MORB would occur as a straight line at 1. Any change in the shape of these lines is ascribed to enrichment processes "effecting their source area or from contamination during their ascent into the crust." (Pearce, 1983, p.234). Pearce (1983) ascribed 5 possible models to explain the variation from the normalized MORB. These are; (1) a subduction zone component in its source, (2) the trace element enriched sub-continental mantle; (3) partial melting; (4) fractional crystallization and (5) possible crustal contamination " (Pearce, 1983, p. 248).

Figure 7 gives a series of Black Hill samples normalized to MORB (Pearce, 1983). 4-201 is a pyroxene monzonite, 5-742 a peridotite, 11-941 a troctolite, 11-1081 an olivine gabbro and BHN-2 the standard from Table 3. This spidergram gives an indication of the range of chemistry exhibited by samples from Black Hill. The peridotite sample is the closest in form to Pearces average MORB. The other samples show progressive patterns of enrichment of K, Rb, Ba, Th and Ce. This trend is comparable to Pearce's crustal contamination curve and is a feature noted in most samples of Black Hill Norite (S.Turner, pers. comm.). Figure 6 shows of samples collected from the mapped area. It shows a roughly straight line with a small peak around Barium. Its linearity suggests a relatively unmodified, mantle derived melt, comparable to Pearce's average tholeiitic MORB. "MORB" in this case refers to a relatively unmodified mantle melt. The single barium peak seems to be anomalous and could be attributed to the mobility of barium in the metamorphic environment or else crustal contamination.

TABLE 2

	A	B	C	D	E
1	elements	898-350	898-369	398-367	bhn-2
2	SiO2	49	49.97	49.77	52.05
3	Al2O3	20.89	14.46	19.23	16.7
4	Fe2O3	7.79	12.24	8.25	10.1
5	Feo	0	0	0	0
6	MnO	0.14	0.23	0.16	0.17
7	MgO	5.63	7.49	6.13	4.77
8	CaO	13.14	11.48	12.44	8.8
9	Na2O	2.38	2.46	2.31	2.73
10	K2O	0.17	0.16	0.24	2.62
11	TiO2	0.88	1.48	0.96	1.31
12	P2O5	0.07	0.13	0.09	0.48
13	SO3	0.02	0.03	0.01	0
14	LOSS	0.18	0.05	0.42	0.25
15	TOTAL	100.28	100.18	100	99.98

	A	B	C	D	E
1		898-350	898-369	898-367	bhn-2
2	Sr ppm	132	122	134	573
3	Rb ppm	7.9	5.1	6.9	150
4	Y ppm	19.3	31	25	26
5	Zr ppm	47	68	57	116
6	Nb ppm	1.9	3.9	2.4	11
7	Ba ppm	33	47	297	615
8	Sc ppm	29	43	36	28
9	Ni ppm	63	69	78	40
10	V ppm	208	344	228	269
11	Cr ppm	155	117	237	
12	Ga ppm	17	19	17	
13	Ce ppm	14	22	13	63
14	Nd ppm	8	9	9	40
15	La ppm	6	0	7	

FIGURE 7

FIGURE 6

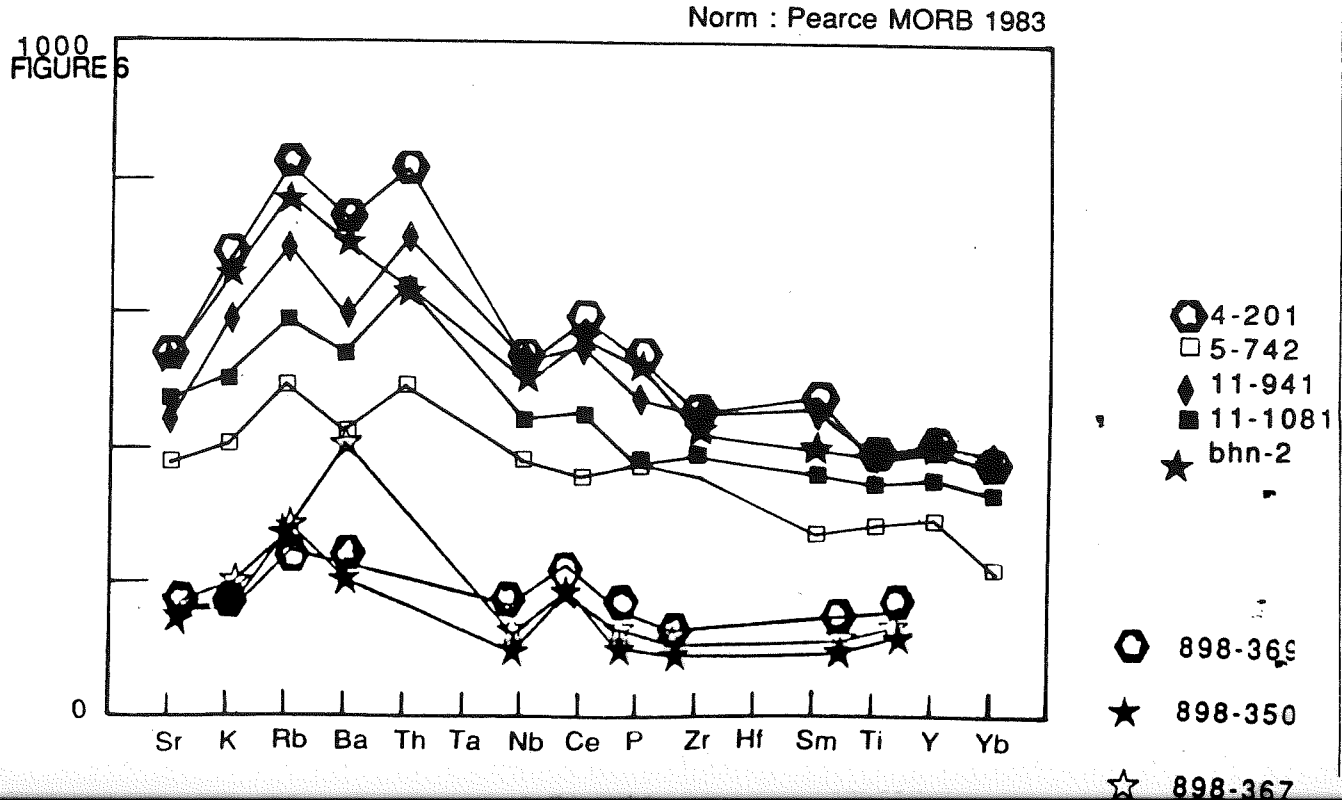

The fact that this outcrop is a very small intrusion and has been chilled implies it would have had little opportunity to assimilation , thereby essentially retaining it's primary character. This seems to be implied by the geochemical data presented. If so, the outcrop may be of great value as representing an initial magma composition for the Black Hill complex, which itself has been involved in extreme assimilation during its emplacement (S.Turner, pers. comm.).

5.3 LEUCOGABBRO

A small outcrop of leucogabbro occurs between the biotite schist and the biotite/epidote gneiss to the east of the major syncline. Randomly orientated amphibole laths indicate that it is undeformed. Microprobe analyses shows the rock to be composed of oligioclase and calcic actinolite. Lithologies texturally similar to this have been found intruding the Reedy Creek granite and the Tanunda Creek Gneiss (S.Turner, pers.comm.; Chinner, 1988), although with somewhat more anorthitic plagioclase compositions of between (An_{44}) and (An_{80}). Field relations show all these rocks to be associated with the major granites or granitic gneisses in the respective areas. This is probably as far as the correlation between the areas can be taken with the meagre amount of evidence available. However further work could be undertaken to explore the possibility of the intrusive/granite/gneiss association being structurally related, that is the possibility of the intrusives having preferentially exploited structural weaknesses in the crust left after the intrusion of the granites.

5.4 CONCLUSIONS

The gabbronorite is correlated to Black Hill complex outcropping on the Murray Plains. This is evidenced by petrology whilst geochemistry implies that it possibly represents a more primary magma composition than is currently recorded from Black Hill. The leucogabbro is, in part, able to be correlated to a variety of leucogabbros associated with granites and granitic gneiss of the Kanmantoo sequence. These non deformed intrusives were clearly sources of heat to the area at the end of deformation. Correlation with similar bodies in the region suggest them to be part of a suite of gabbroic bodies related to a thermal event (See chapter 7) and possibly related to a mild terminal extensional phase in the Delamerian Orogeny (Foden et al., in press).

6. METAMORPHISM

6.1 INTRODUCTION

The region around Springton has been metamorphosed to upper amphibolite facies. The mapped area is entirely within migmatite grade, placing it in the highest grade of metamorphism in the Kanmantoo. A general model of the type of metamorphism in this region has been proposed by Sandiford et al .(in press) who conclude that the style of metamorphism is a low pressure, high temperature Buchan style metamorphism characterised by the existence of andalusite/sillimanite assemblages.

6.2 AMPHIBOLE-PLAGIOCLASE EQUILIBRIA

The partitioning of Na between plagioclase and amphiboles is a direct response to temperature and pressure conditions at the time of equilibrium. Indeed, theoretically it is possible to delineate a metamorphic series as an expression of this partitioning with changing pressure and temperature conditions (Spear, 1981). Observations from a great number of terrains indicate plagioclase becomes more calcic with increasing metamorphic grade and amphiboles become more sodic and aluminous. The empirical model relating this partitioning to metamorphic grade has been devised by Spear (1981) and has been used on rocks of differing ages from this area. The mass transfer reaction

$$NaAlSi_3O_8 + \#Ca_2Mg_5Si_8O_{22}(OH)_2 = NaCa_2Mg_5\overset{Al}{\underset{\wedge}{}}Si_7O_{22}(OH)_2 + 4SiO_2 \qquad (1)$$

albite tremolite edenite quartz

describes the variation in A-site occupancy of the amphibole with plagioclase composition. This reaction proceeds to the right with increasing metamorphic grade. The equilibrium constant, **K**, will also increase with increasing metamorphic grade. This constant is represented as :

$$\mathbf{K} = a_{am,ed}/a_{am,tr}.a_{pl,ab} \qquad (2)$$

A related discontinuous reaction:

$$\text{actinolite} + \text{albite} = \text{hornblende} + \text{anorthite} + \text{quartz} \qquad (3)$$

also proceeds to the right with increasing metamorphic grade. Spear (1981) deduces the activities of both amphiboles and albite as functions of there compositional variations and activity coefficients "assuming ionic solid solution, local charge balance and identical site occupancy of M1 and M3 sites in the amphiboles." (Spear, 1981, pg 357). Thus the activity of albite is represented by:

$$a_{pl,ab} = X_{ab} \cdot \gamma_{ab}$$

The activity of tremolite by:

$$a_{am,tr} = (X_{\square,A}\gamma_{A}).(X_{Ca,M4}\gamma_{Ca,M4})^2.(X_{Mg,M1+M3}\gamma_{Mg,M1+M3})^3.(X_{Mg,M2}\gamma_{Mg,M2})^2$$

and the activity of edenite by:

$$a_{am,ed} = (X_{Na,A}\gamma_{Na,A}).(X_{Ca,M4}\gamma_{Ca,M4})^2.(X_{Mg,M1+M3}\gamma_{Mg,M1+M3})^3.(X_{Mg,M2}\gamma_{Mg,M2})^2$$

The equilibrium constant for (1) can be written as a function of compositional variation and activity coefficients:

$$K = (X_{Na,A}/X_{\square,A}\ X_{ab})\cdot\gamma_{Na,A}/\gamma_{\square,A}\ \gamma_{ab}$$

It is noted that both plagioclase and amphiboles exhibit non-ideal solid solution and this is indicated by the miscibility gaps that open up at significant temperatures and pressures. Therefore values of the ideal equilibrium constant $\mathbf{K_{(id)}}$ are strongly compositionally dependent (Spear, 1981). Also amphiboles from quartz bearing amphibolites "equilibrated at high pressures should have larger A=site occupancies than amphiboles crystallized at lower pressures and equivalent temperatures" (Spear, 1981, pg.362). This is particularly relevant to such equilibrium assemblages in the mapped area as they have crystallized at a low pressures appropriate to Buchan style metamorphism (Sandiford et al., in press) and therefore would have smaller A-site occupancies.

Since the activity models for amphiboles and plagioclase are imprecisely understood we can only use qualitative methods. Qualitatively the change in grade by this systematic partitioning of Na and amphibole A-sites can be represented by plotting $X_{(Ab)}$ vs $X_{(Na).A}$. $X_{(Na).A}$ is calculated as $X_{(Na)}/X_{(Na)} + X_{\square,A})$ where $(X_{\square,A})$ is equal to $1-X_{Na,A} - X_{K,A}$. Phase

diagrams are possible because tremolite, edenite, quartz and albite are co-planar. Thus by projecting from quartz a phase diagram is created with albite, edenite and tremolite forming the base of the triangle and anorthite the apex (Figure 8). This triangle is then skewed into a rectangle for ease of representation. Tie lines represent systematic partitioning of Na and A-sites and with increasing grade, becoming progressively steeper. A general representation of these diagrams from lower greenschist to upper amphibolite facies is given in Figure 9. This group of diagrams show distinct changes in topology, in particular the co-existence of more calcic plagioclase with more sodic and aluminous amphiboles. This systematic partitioning is strong evidence for equilibrium crystallization.

In the Springton area, data sets from the calcsilicate gneiss, the Rathjen gneiss, the amphibolite, the amphibole intrusive and the gabbronorite have been used to establish the plagioclase-amphibole equilibria. Figure 10A-G show the phase diagrams appropriate for the rocks.The calcsilicate gneiss in phase diagram A shows plagioclases of an albite/oligioclase composition and amphiboles of a tremolite composition. Textures suggest they are in equilibrium but Figure 10A shows a lower grade of metamorphism than would be expected in this area. This is attributed to the highly non ideal relationship of $X_{Na(A)}$ and will be dealt with later. The crossed tie lines in B, C, G, E, and F are the result of relict igneous phases and metamorphic reactions. The Rathjen gneiss in 10B shows amphibolite grade metamorphism which is the grade expected in this area. In 10C the amphibolite dyke shows high grade metamorphism with plagioclase of an oligioclase/andesine composition and amphiboles with around 0.6 Na substitution. This is equivalent to upper amphibolite facies, the slope of the tie lines being steep and the geometry of the phase diagram similar to that of the general model presented in figure 9. Figure 10D shows a very low grade association of albite and tremolite in the leucogabbro. This is either the result of the initial igneous association or the highly non-ideal nature of the components and will be discussed later in this chapter. The prevalence of anorthite rich plagioclase coexisting with varying amphibole composition is diagnostic of a rocks igneous character as much as its metamorphic one. In 10D the slope of the tie lines are indicative of upper amphibolite facies according to the schematic classification in Figure 9 and the crossed tie lines indicate a relict igneous association. Fig. 10D and 10E are of the same

Figure 8 Phase diagram showing idealized relationship of amphiboles and plagioclase

Figure 9 Schematic phase representation of X_{Ab} in plagioclase vs. $X_{Na.A}$ in amphiboles with increasing metamorphic grade. (after Spear, 1981).

9A Chlorite zone (lower greenschist facies)

9B Chlorite-biotite zone (Lower greenschist facies)

9C Oligoclase isograd (middle greenschist facies)

9D Garnet-oligoclase zone to staurolite isograd (Greenschist-amphibolite facies transition?)

9E Staurolite zone (amphibolite facies)

9F Sillimanite zone (upper amphibolite to granulite facies)

FIGURE 8

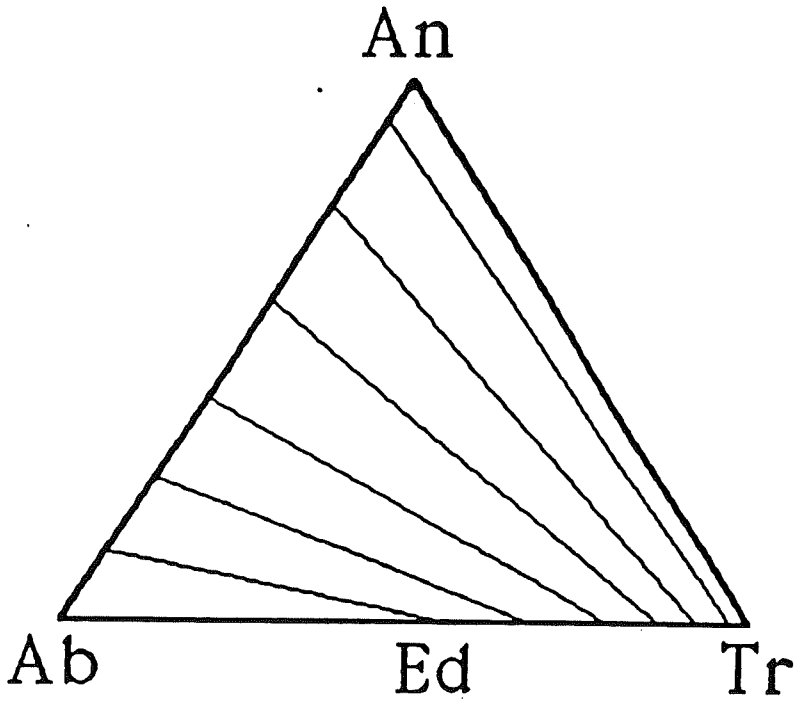

FIGURE 9

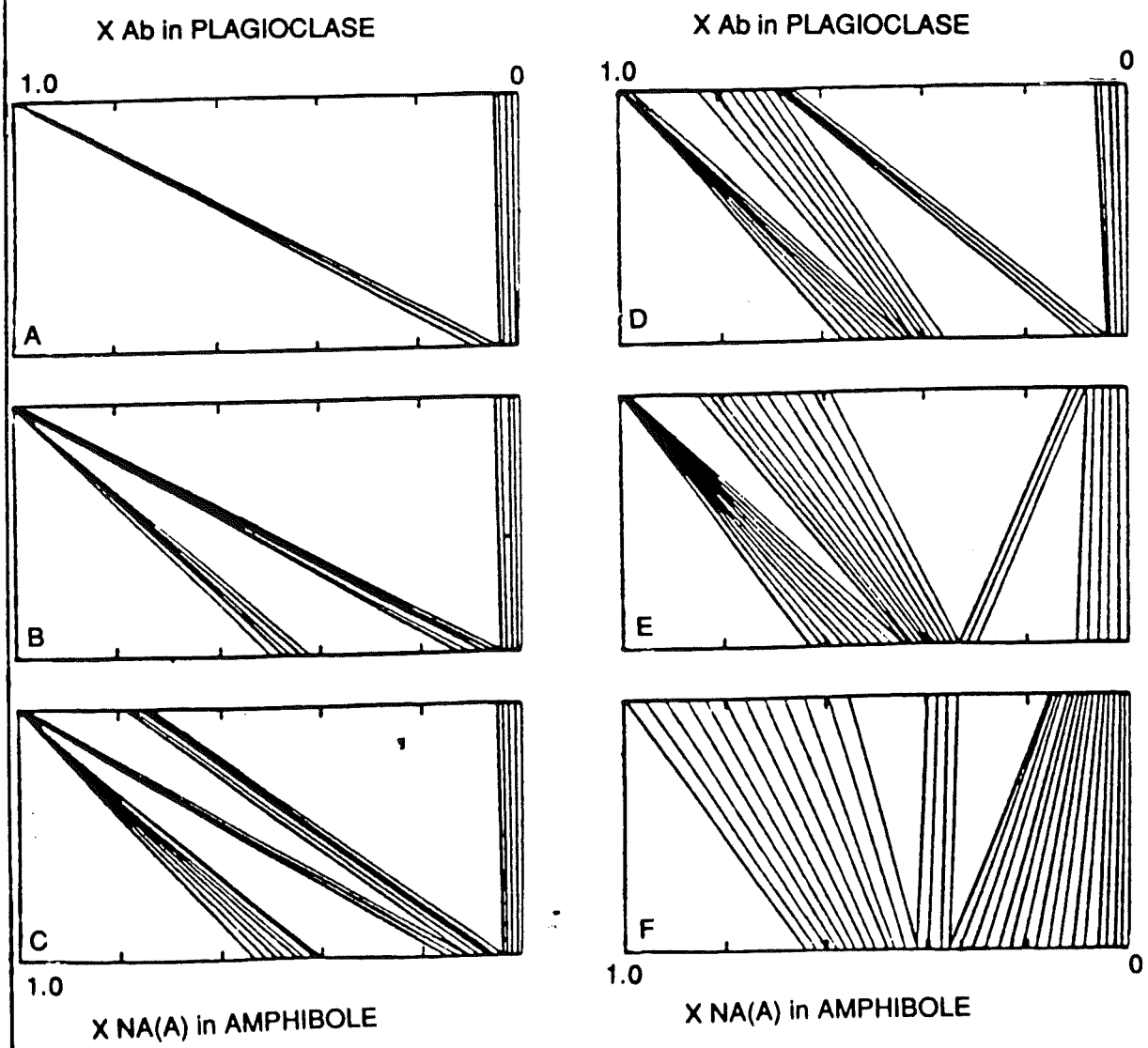

lithology. Figure 10D is almost identical to the general model presented for upper amphibolite facies. Using the qualitative temperature X_{Ab} vs. $X_{Na(A)}$ diagram of Spear (1981) (Figure 11), temperatures of between 350° and 740° are determined for these rocks. The rocks that show upper amphibolite facies from the phase diagrams, e.g. the Rathjen gneiss, the amphibolite dyke and the porphyritic gabbronorite all show higher temperatures from this geothermometre than the calcsilicate and the leucogabbro. To constrain pressure, a geobarometre defined by the alumina contents of amphiboles (Hollister et.al., 1987) was employed (Table 5). Average pressures range from 1 kbar to 4.4 kbar, consistent with the results of Sandiford et. al. (in press).

6.3 INTERPRETATION OF DATA

The highly non-ideal nature of amphibole -plagioclase equilibria in these rocks does not enable any precise quantitative evaluation of the pressure/temperature controls. Consequently the errors associated with the above pressure and temperature estimates must be extremely large. However certain qualitative contraints can be discerned. From the above section temperatures, on average, were constrained to around 700° and pressures were less than about 5 kbars. However the calcsilicate in particular shows variation within this trend. Above 700°C plagioclase shows complete solid solution between anorthite and albite. Below this temperature, a number of miscibility gaps appear. They are classified as the Hunttenlocher (An_{60}-An_{90}), Boggild (An_{45}-An_{60}), Voll (An_{40}-An_{90}), and peristerite (An_{0}-An_{14}) miscibility gaps (Spear, 1981). Apart from the obvious difference between relict igneous and metamorphic plagioclase compositions, there is still evidence of immiscibility in these rocks (Figure 12). The ramification of these miscibility gaps is that in Na rich assemblages, Na will be retained in plagioclase over a greater range of temperatures than expected for the ideal behaviour. Oba (1980) has shown that miscibility gaps are also highly pressure sensitive. At low pressures e.g. 1-2 kbars complete miscibility may never be achieved. Therefore Na may be retained in plagioclase during low pressure metamorphism independently of the temperature. This response allows high Na plagioclase compositions in a region that has been metamorphosed at high temperatures and low pressures. Likewise amphibole A-sites occupancies will be smaller in rocks crystallized at lower pressures than those crystallized at

Figure 10 Schematic phase representation of X_{Ab} in plagioclase vs. $X_{Na.A}$ in amphiboles with increasing metamorphic grade. (after Spear, 1981).

10A 898-319 Calcsilicate gneiss

10B 898-309 Rathjen gneiss

10C 898-358 Amphibolite

10D 898-306 Leucogabbro

10E 898-350 Gabbronorite

10F 898-368A Porphyritic Gabbronorite

10G 898-368B

FIGURE 10

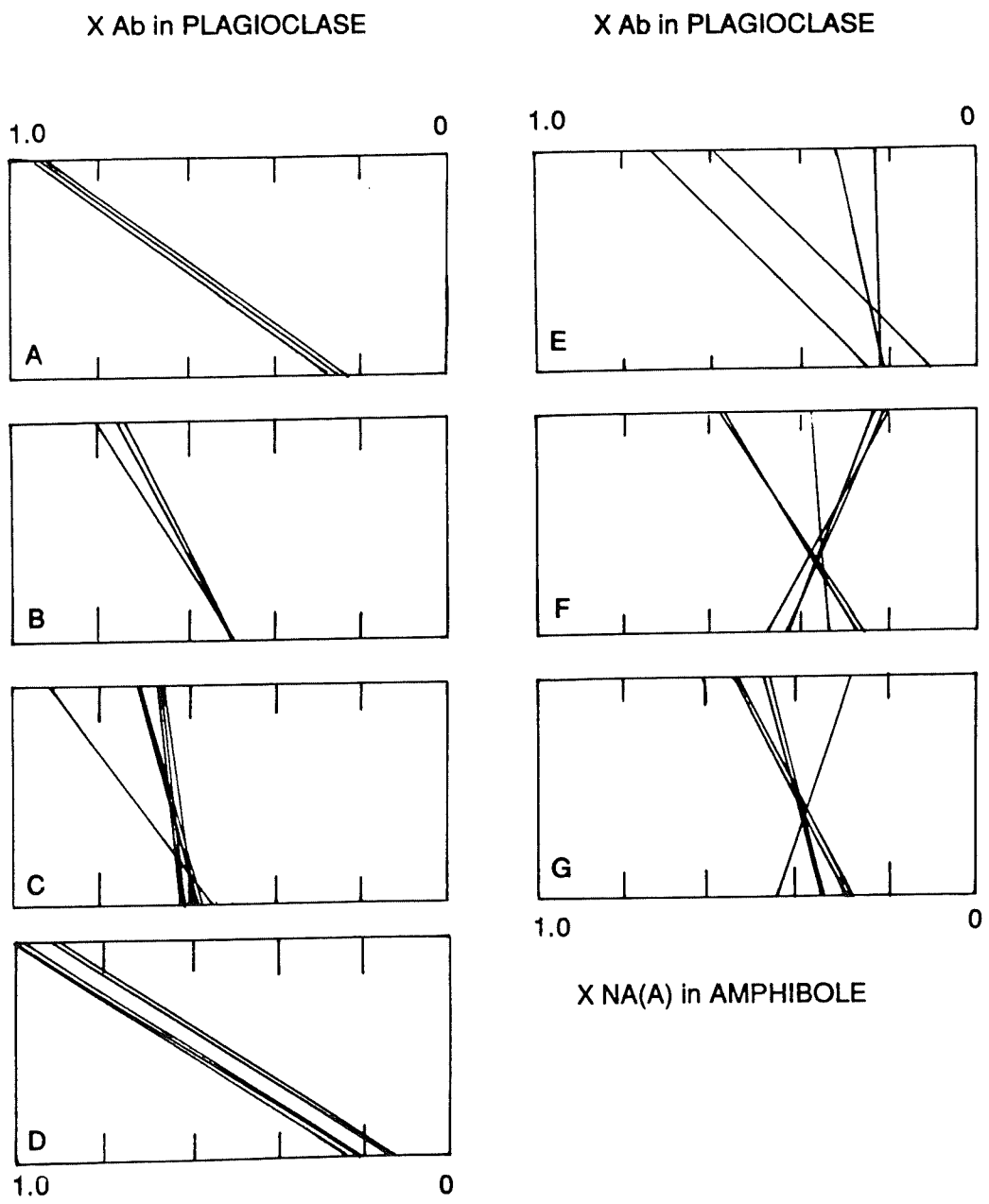
X Ab in PLAGIOCLASE
1.0
0
A
B
C
D
1.0
0
X NA(A) in AMPHIBOLE
X Ab in PLAGIOCLASE
1.0
0
E
F
G
1.0
0
X NA(A) in AMPHIBOLE

higher pressures and equivalent temperatures (Oba, 1980). These observations are consistent with low Na amphiboles coexisting with Na rich plagioclase in assemblages metamorphosed at high temperatures and low pressures and provide a possible explanation as to why the calcsilicate gneiss shows such seemingly low grade assemblages when compared with Rathjen gneiss.

6.4 CONTROLS ON MELTING IN PELITIC MIGMATITES

The presence of migmatites in this area indicates at the peak of metamorphism partial melting commenced. This section will discuss the controls on this melting using mineral chemical compositions from electron microprobe data.

The type of migmatites in this area are of the stromatic or layered variety after Mernhert (1971). Nomenclature of the various zones within these migmatites are also taken from Ashworth (1985) after Mernhert (1971). The term leucosome is used to describe the felsic melt fraction which generally exhibit coarsest grainsize. The term melanosome will be used to describe the mafic selvage that rims the felsic layers. These represent unmelted biotites. The term mesosome will be used to describe the undifferentiated part of the rock and thus the unmelted portion of it. Biotites from melanosomes, mesosomes and leucosome of the migmatites were probed as were biotites from the Rathjen gneiss and the biotite schist for comparison. The results of these analyses are represented in Appendix 2.

The Mg vs Fe content of the leucosome and mesosome of migmatite 898-360 are recorded as Figure 13. There is an obvious difference in the compositon of melted (B) and unmelted (A and C) biotites, the melted ones having an average 6-5% higher magnesium content than the unmelted ones. This is perhaps a little unusual as Fe would be expected to substitute for Mg with increasing temperatures. The most likely explanation of this result is that the biotites had an already high Mg content before melting, that is, the melting was compositionally dependent though consistent with low pressure melts. Figure 14 is a plot of the Fe vs.Mg content of the Rathjen gneiss, the biotite schist and the migmatites. These show the unmelted biotites of the migmatites to be almost identical to those of the biotite schist

Table 3 Pressues in k bars of rocks in the mapped area after Hollister et al., 1987.

898-319 Calcsilicate gneiss

898-309 Rathjen gneiss

898-358 Amphibolite

898-306 Leucogabbro

898-350 Gabbronorite

898-368A Porphoritic Gabbronorite

898-368B

"neg" refers to pressure values that computed negative from the technique used.

Figure 11A Plot of $X_{Na,A}$ in amphiboles vs. X_{Ab} in plagioclase of rocks from Figure 10. Hypothetical Temperature contours after Spear (1981).

11B Depicts contours of constant K_{id} (after Spear, 1981).

FIGURE 11

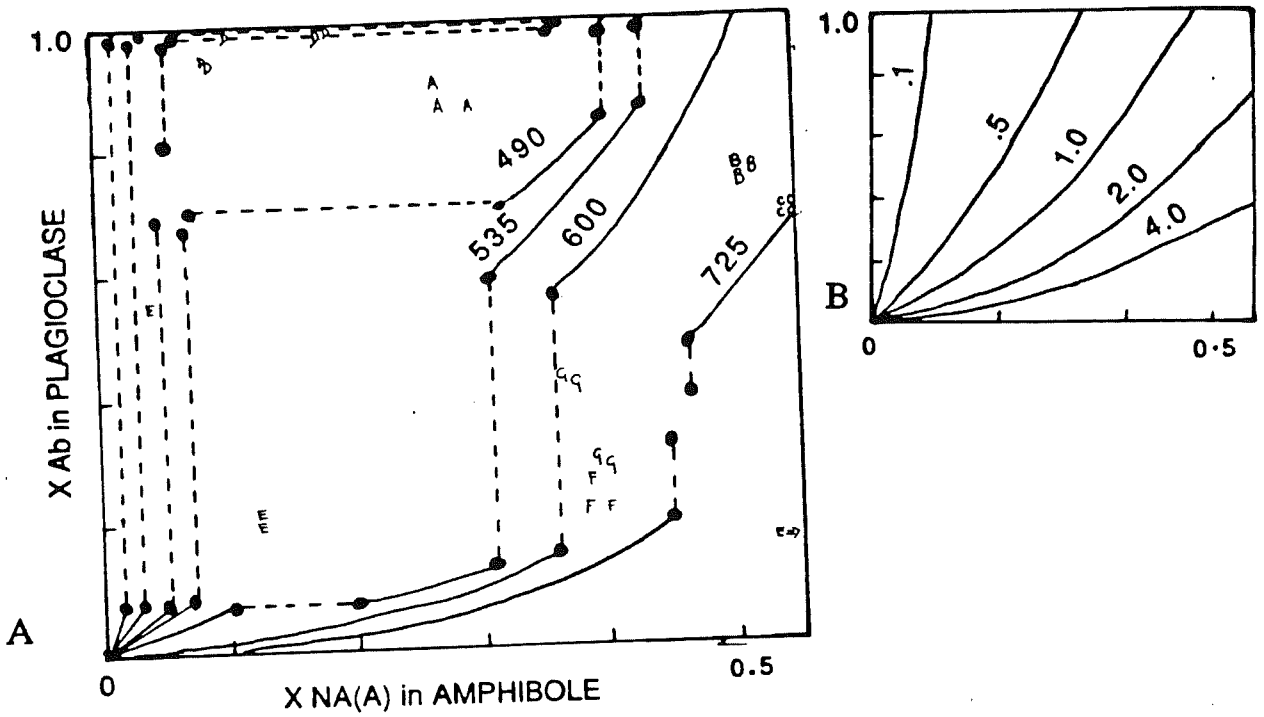

A 898-319 Calcsilicate gneiss

B 898-309 Rathjen gneiss

C 898-358 Amphibolite

D 898-306 Leucogabbro

E 898-350 Gabbronorite

F 898-368A Porphyritic Gabbronorite

G 898-368B

TABLE 3

898-319	989-309	898-358	898-306	898-350	898-368a	898-368b
neg	4.18	3.75	neg	7.23	3.58	3.78
neg	5.3	3.68	neg		5.88	3.54
neg		4.05	neg		3.51	4.14
		4.35			3.75	4.4
		4.44			1.71	4.14
		4.5			1.53	3.99

which confirms field evidence (see Chapter 2) that they are indeed phases of the same lithology, varying only in Mg:Fe ratio with the onset of melting.

6.5 CONCLUSIONS

Amphibole-plagioclase equilibria can be used to constrain temperatures in metamorphic terrains that do not have any other suitable geothermal indicators (Spear, 1981). Likewise amphibole Al content is a possible geobarometre (Hollister et al., 1987). The maximum metamorphic temperatures of ~700° at pressures < 5 kbars in the mapped area are consistent with those of other workers (e.g.Sandiford et al., in press). However the amount of variation within these results suggests that this comparison is somewhat tenuous. The results from melted biotites indicates the melting of pelitic migmatites is compositionally controlled and these results support the genetic models of the Rathjen gneiss and the biotite-rich metasediments proposed previously.

Figure 12 Depicts miscibility gaps within plagioclase

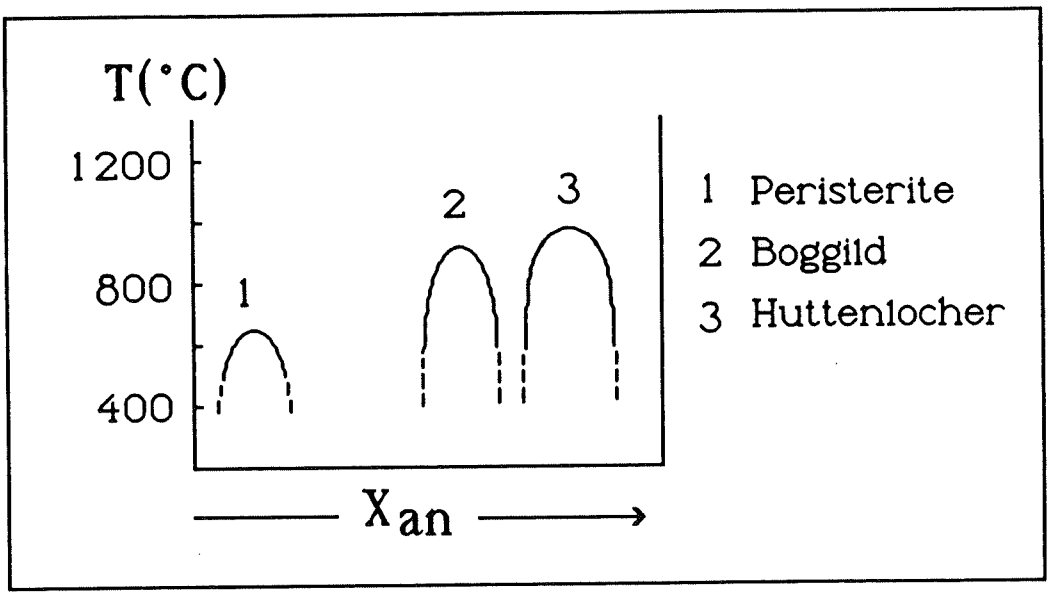
T(°C)
1200
800
400
1
2
3
Xan
1 Peristerite
2 Boggild
3 Huttenlocher

Figure 13A Depicts FeO Vs. MgO in biotites from migmatites

898-360A is from the melanosome

898-360B is from the leucosome

898-360C is from the mesosome

Figure 13B Depicts Fe2+ vs. Mg2+ in biotites from migmatites.

898-360A is from the melanosome

898-360B is from the leucosome

898-360C is from the mesosome

FIGURE 13

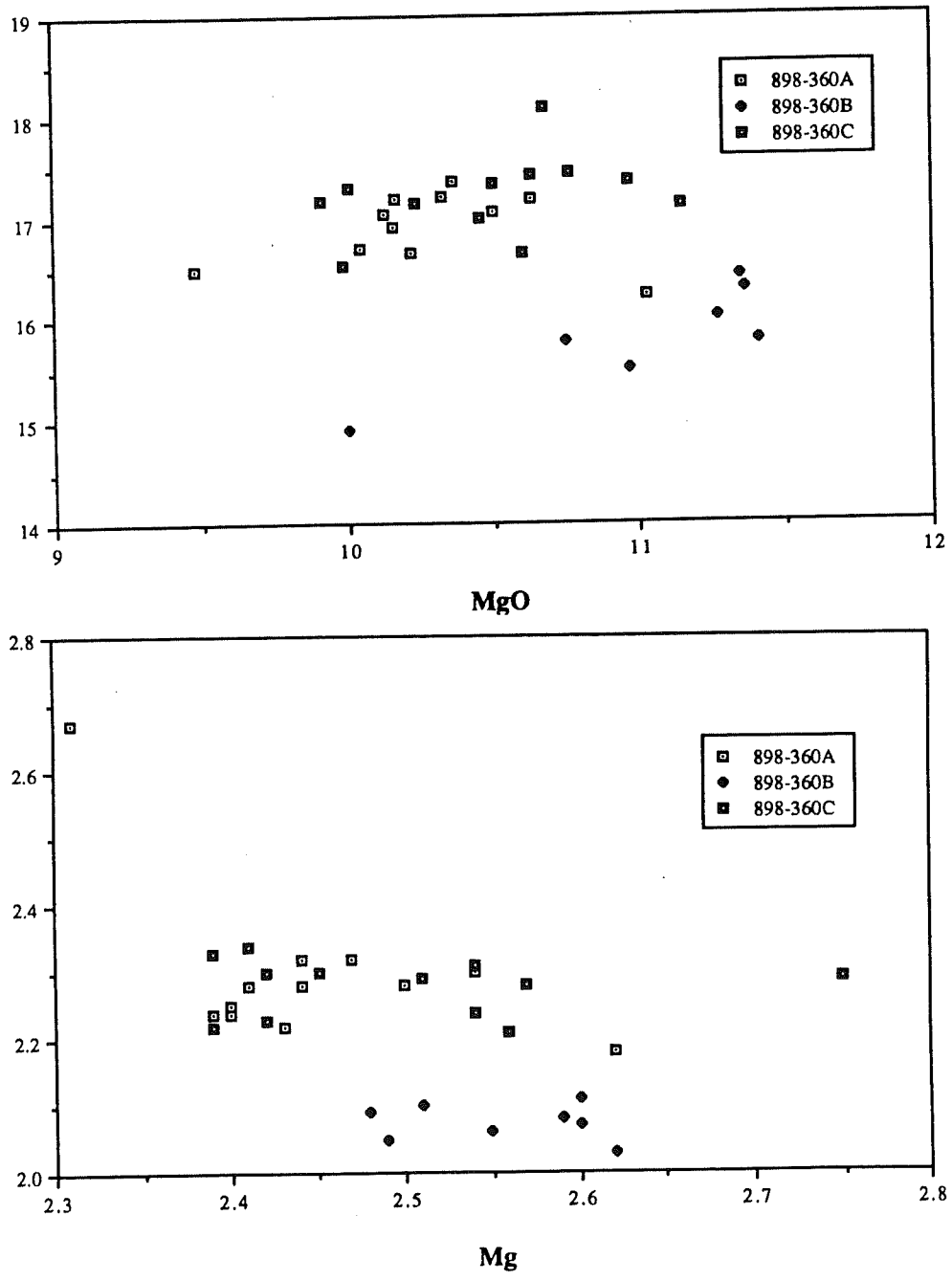
19
18
17
16
15
14
9
10
11
12
MgO
898-360A
898-360B
898-360C
2.8
2.6
2.4
2.2
2.0
2.3
2.4
2.5
2.6
2.7
2.8
Mg
898-360A
898-360B
898-360C

Figure 14A Depicts Fe2+ vs. Mg2+ in biotites from migmatites, biotite scist and the Rathjen gneiss

898-360A is from the melanosome

898-360B is from the leucosome

898-362 is the biotite schist

898-309 is the Rathjen gneiss

14B Depicts FeO vs. MgO in biotites from migmatites, biotite scist and the Rathjen gneiss

898-360A is from the melanosome

898-360B is from the leucosome

898-362 is the biotite schist

898-309 is the Rathjen gneiss

FIGURE 14

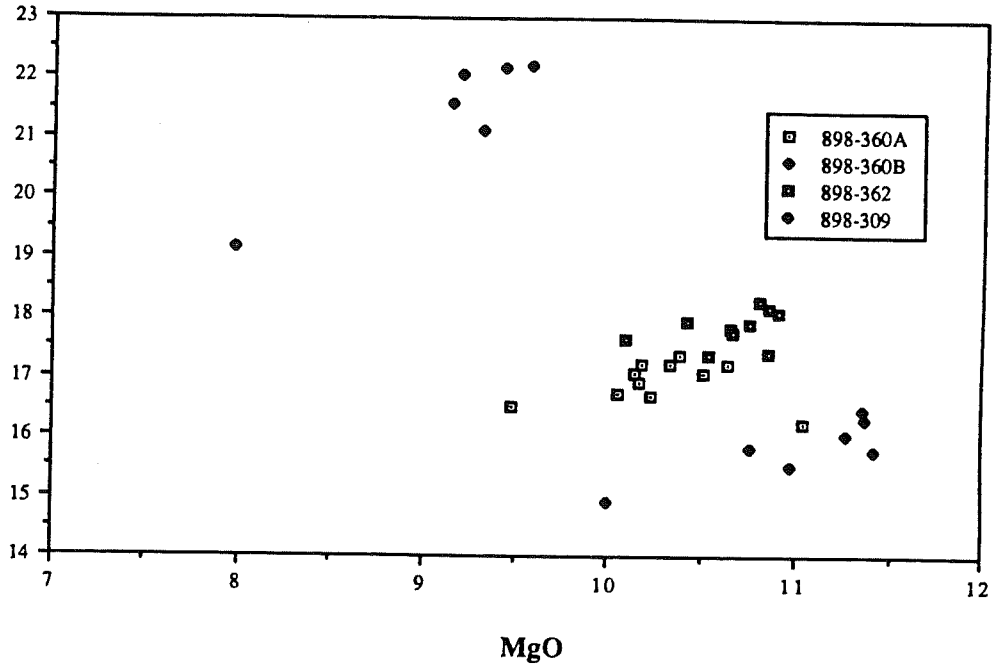
23
22
21
20
19
18
17
16
15
14
7
8
9
10
11
12
MgO
898-360A
898-360B
898-362
898-309

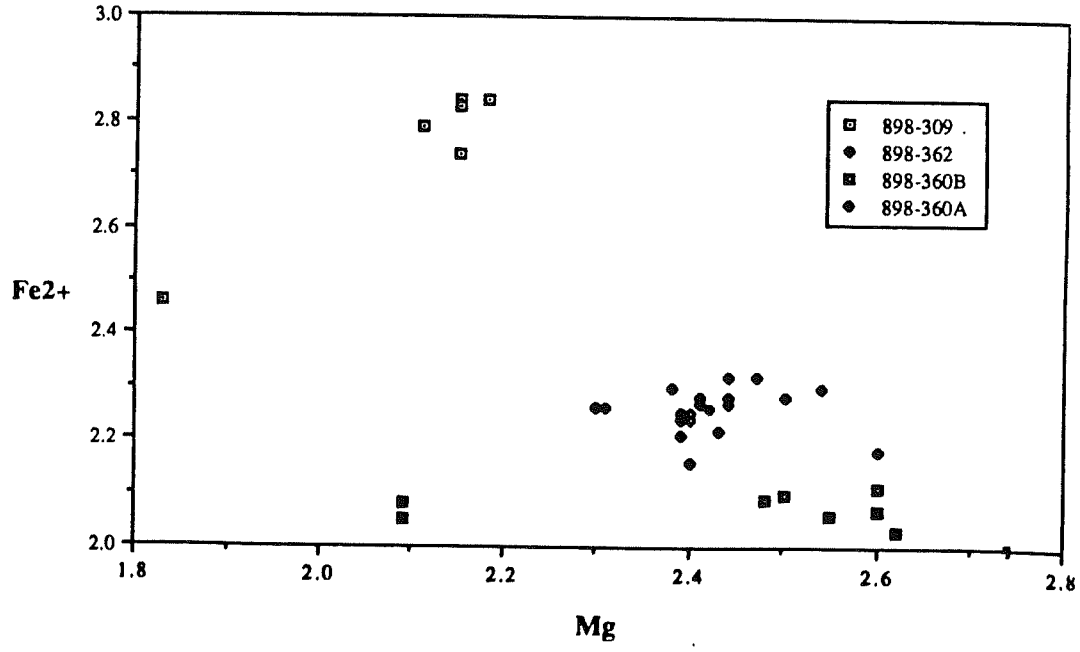
3.0
2.8
2.6
2.4
2.2
2.0
1.8
2.0
2.2
2.4
2.6
2.8
Fe2+
Mg
898-309
898-362
898-360B
898-360A

7. GEOLOGICAL SYNTHESIS

7.1 INTRODUCTION

In considering metamorphic terrains and on a larger scale, orogenic belts, certain fundamental concepts should be addressed if a viable model is to be conceived. These include how the rocks have reached the observed metamorphic temperatures (the thermal budget of the region), why they were deformed (deformational and thermal considerations) and the overall mass budget of the area (including deformational, metasomatic and erosional considerations). Questions such as "Where did the heat come from?", "How deep were the rocks buried?" and "What is the relationship between deformation and metamorphism?" must be addressed if any regional model is to be conceptualized.

One of the aims of this thesis was to try and document a more general metamorphic and deformational model for the region based on specific parametres such as the structural relationship of the Rathjen gneiss to the host sediments, amphibole-plagioclase equilibria of rocks of different ages and the controls of melting in pelitic migmatites. In this chapter, an interpretation is made considering the fundamental concepts discussed previously and from the constraints observed from the specific parametres.

7.2 A RELATIVE CHRONOLOGY OF DEFORMATION AND METAMORPHISM IN THE KANMANTOO.

A diagramatic representation of the relative timing of deformation and metamorphism is presented in Figure 15. After deposition of the sediments the Rathjen gneiss was intruded. With the heat produced from this intrusion localized metamorphism and melting commenced. The Delamerian Orogeny then commenced with an early N-S tectonic movement of the orogenic belt as represented by the stretching lineations within various competent lithologies, especially the Rathjen gneiss, and F_1 isoclinal folding. The presence of F_1 leucosomes is attributed to the localized melting of sediments during the intrusion of the Rathjen gneiss. Intrusion of mafic dykes such as the amphibolite also occurred coeval with F_1 as demonstrated by a predominantly N-S trending stretching lineation. Metamorphism reached a climax

Figure 15 Relative chronology of deformation and metamorphism around Springton

FIGURE 15

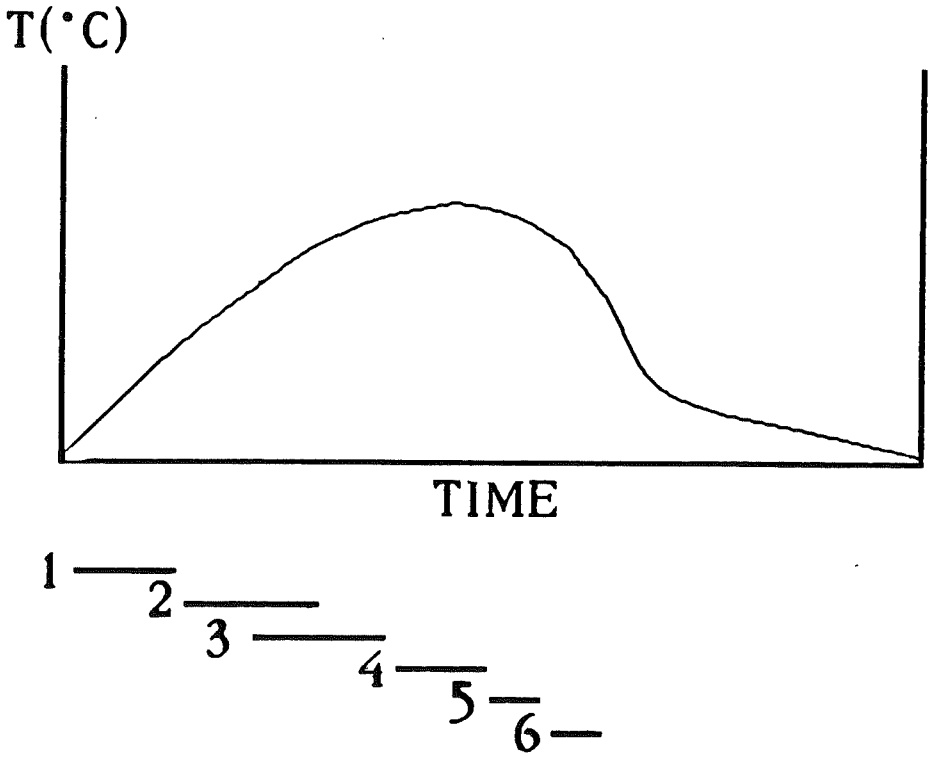

1. Sedimentation
2. Intrusion of Rathjen Gneiss
3. D_1 deformation
4. D_2 deformation
5. D_3 deformation
6. Intrusion of Black Hill Norite

between F_1 and F_2 reaching upper amphibolite facies evidenced by the F_2 folds folding sillimanite in the biotite schist. F_2 indicates a changing in the relative motion of the Foldbelt, from N-S to E-W. By F_3 metamorphic temperatures were waning though the emplacement of post deformational intrusives high in the crust would have certainly maintained the thermal budget for some time after the cessation of deformation. The fact that the gabbronorite has a chilled margin is indicative that it intruded into significantly cooler rocks. However these intrusions would have lost most of their effective regional heat by the time they reached the upper crust and therefore the metamorphism was not sustained for any great time.

It can be observed from this relative chronology that the metamorphism formed a continuum throughout the Delamerian Orogeny. The span of this metamorphism is inately associated with the chronology of both intrusion and deformation. Therefore any regional model of deformation and metamorphism must account for this observed affinity.

7.3 SIGNIFICANCE OF THE STRETCHING LINEATION AT SPRINGTON

In the past, it has been argued that the structures developed in deformed zones of continental crust could not be used in any accurate way to determine directly the nature of plate motion across the deforming zone. However recently studies have shown that continental structures, in particular stretching lineations accurately reflect the relative direction of lithospheric plate motion across such deformed zones. Data from diverse orogenic belts, including the Variscan, the Caledonian, the Himalaya and north east Africa indicate that stretching lineations accurately reflect the known plate motion (Shackleton and Ries, 1984). This is because orogenic belts can be conceived as "shear zones on a crustal scale" and that this "shear zone geometry involves extension in or close to the direction of shear" (Shackleton & Ries, 1984). As a consequence of this recent enlightenment we now understand that stretching lineations and associated structures in orogenic belts provide an invaluable key to the understanding the plate tectonic evolution of orogenic belts. Therefore the N-S trending stretching lineation within the Rathjen gneiss and other competent lithologies is quintessential to the understanding of plate motion during the Delamerian Orogeny.

7.4 THERMAL CAUSES OF BUCHAN ZONE METAMORPHISM AT SPRINGTON

From various qualitative parametres already documented in the preceding chapters, the maximum temperatures reached during metamorphism were approximately 700°C whilst maximum pressures were less than 5 kbars The fundamental question is "How did such high temperatures occur at such low pressures?" As the NE Scottish Dalradian Buchan metasediments show similarities to E Mt Lofty Kanmantoo metasediments in terms of tectonic and metamorphic setting, comparative thermal models are possible.

The first model is that of discrete intrusions whose thermal effects combined with the thermal effects of tectonically thickened crust are responsible for the regional metamorphism. In NE Scotland, Chinner(1967) sees the Buchan style metamorphism as the result of a thermal anticline at depth. The cause of this anticline is attributed to the elevation of isotherms by the upward movement of convecting material during deformation. As this anticline is positioned in the hinge zone of the Tay/Banff nappe this is interpreted as an indication of a tectonic contribution to heat flow at higher areas of the crust. To apply this model to the E Mt Lofty Ranges is very successful as metamorphic temperatures are too high to be attributed to crustal thickening alone. The presence of the gabbronorite and regionally, Black Hill Norite would have increased the thermal budget of the area significantly to attain these temperatures.

Similarly Harte and Hudson(1979) maintain regional metamorphism in E.Scotland is the result of the emplacement of a regional magma. Therefore at the time of metamorphism the geothermal gradient was convex to the Temperature axis. They have attributed the control of this geotherm to a regional magma source at depth with the height this source intruded into the crust controlling the local variation in the metamorphic pattern. In the E Mt Lofty Ranges the emplacement of a mantle derived magma such as Black Hill Norite is an analogous situation.

A model of simple crustal thickening and concurrent erosion being responsible for Buchan style metamorphism is proposed by Richardson and Powell in E Scotland (1976). They maintain that by tectonically thickening the crust, the radioactive elements present are increased proportionally to the rate of tectonic thickening within the orogenic belt. The "thermal inertia of the upper crustal rocks during metamorphism is offset by concurrent erosion" (Richardson and Powell, 1976). The effect of erosion is necessary to decrease the depth of the geothermal gradient continually in the crust. They maintain that the temperatures

reached by this tectonic thickening with slight input from basement rocks are sufficient to produce the observed Buchan style metamorphism and therefore need not require an external heat source. In the E Mt Lofty Ranges the style of folding suggests that there is tectonically thickened crust, though that this is sufficient to produce the observed metamorphism is unlikely.

The final thermal model maintains that an unknown or undetectable mechanism such as a fracture at the base of the crust is responsible for the observed metamorphism (Turner,1980). Turner maintains that the amount of heat required to drive Buchan metamorphism and actually take to completion all the endothermic dehydration and decarbonation reactions from an initially cool pile of rocks is vast. Therefore the emplacement of a series of plutons is thermally insignificant to do so. Turner (1980) sees the emplacement of the syn Dalradian plutons as symptomatic of thermal conditions rather than the cause of it. Thus both the regional metamorphism, the emplacement of granites and the presence of migmatites represent the culmination of some thermal perturbation of the deeper crust or mantle. In the E Mt Lofty Ranges this is a possibility although the presence of mantle derived magmas indicate that there was a readily observable heat source available to cause the high temperature metamorphism.

7.5 CONCLUDING DISCUSSION

The tectonic history of the Kanmantoo group is one of intrusion, metamorphism and deformation. The mineral assemblages in the area are indicative of severe thermal perturbations in the vicinity of Springton during the Delamerian Orogeny. The thermal causes of this metamorphism is associated with both crustal thickening and the intrusion of a regional magma. The Rathjen gneiss not only reflects the metamorphism of the area through amphibole-plagioclase equilibria but also the direction of tectonic transport early in the history of the Delamerian Orogeny. N-S stretching lineations preserved in it enable the direction of relative plate motion to be discerned. The intrusive nature of the Rathjen gneiss also enables a possible tectonic setting to be determined. Therefore the Rathjen gneiss is capable of providing

many of the keys to a further understanding of the tectonic history of the KanmantooGroup during the Delamerian Orogeny.

ACKNOWLEDGEMENTS

Mike Sandiford has been a constant source of enthusiasm and wonder throughout the year and I would have been lost without his supervision, accessability and friendship. I would also like to thank Larry Frakes and John Foden for giving me the oppurtunity to do this course and Robin Oliver, Richard Jenkins and Alan Purvis for discussions and papers related to my topic throughout the year.

Acknowledgement is made to the technical staff- Geoff Trevellyan, Wayne Mussared, Ric Barrett, Sherry Proferes and John Willoughby for all their help during the year and to Hew and Vanessa for their patience with me and the electron microprobe. Also to Leon and Leonie Holmes at Springton for use of their property during my mapping project.

Much love and thanks must be extended to Simon Turner, Kathy Stewart and Kim Hein for their never ending advise, assistance, friendship and fun. To Simon, many thanks for the recommendations on the text also. Thanks must be given to Michelle and Chris for their generosity and accommadation. Emotional stability provided by 5MMM fm and The Go-Betweens.

To the other Honours students (my boys); Chris, Andrew, Peter, David, James and Marius; thanks for the love, gossip, sanity and insanity. Here's looking to brighter days.

Many thanks to my parents, my brothers Jamie and B.J. and my "sister" Angey for all their love, time and patience throughout the year.

Finally I would like to thank John Weston for showing me just how groovy rocks could be.and Mike as ever, for confirming this particular conceptual reality.

REFERENCES

Allen, R.V.A., 1977: Metamorphic phase relations in the Kanmantoo. Hons. thesis, University of Adelaide (unpubl.).

Ashworth, J.R., (Eds) 1985: Migmatites, Glasgow.

Atherton, M.P., 1977: The Metamorphism of the Dalradian rocks of Scotland. Scott. J. Geol. 13(4) :331-370.

Chappell, B.W., and White, A.J.R., 1974: Two contrasting granite types. Pacific Geology, 8: 173-174.

Chinner, G.A., 1980: Kyanite isograds of Grampian metamorphism. J. Geol. Soc. London, Vol. 137: 35-39

Chinner, G.A., 1967: The distribution of pressure and temperature during Dalradian metamorphism. Q. J. Geol. Soc. London. Vol. 122: 158-186.

Daily, B. and Milnes, A.R., 1973: Stratigraphy, structure and metamorphism of the Kanmantoo Group (Cambrian) in its type section east of Tunkalilla Beach, South Australia. R.Soc.S.Aust., Trans. 97: 213-251.

Deer, W.A., Howie, R.A., and Zussman, J., 1966: An introduction to the rock-forming minerals. London: 529pp.

Dewey, J.F., and Pankhurst, R.J., 1970: The evolution of the Scottish Caledonides in relation to their radiometric age pattern. Trans. R. Soc. Edinb. Vol. 68: 361-389.

Ernst, W.G., 1968: Amphiboles - Crystal Chemistry Phase Relations and Occurrence. U.S.A.: 113pp.

Fettes, D.J., 1979: A metamorphic map of the British and Irish Caledonides. In: Harris, A.L., Holland, C.H., and Leake, B.E., (Eds) , The Caledonides of the British Isles - reviewed. Geol. Soc. London. Spec. Publ. no. 8: 307-319.

Fleming, P.D., and Offler, R., 1968: Pre-tectonic metamorphic crystallization in the Mt. Lofty Ranges, South Australia. Geol. Mag. Vol. 105, No. 4: 356-359.

Fleming, P.D., and White, A.R.J., 1984: Relationships between deformation and partial melting in the Palmer migmatites, South Australia. Aust. J. Earth Sciences 31: 351-360.

Foden, J.D.,Turner, S.P. and Morrison, R.S., in press: Tectonic implications of Delamerian magmatism in south Australia and western Victoria. Geol.Soc.Aust. Spec.Publ. Daily Volume.

Gatehouse, C.G. , 1988: Kanmantoo Field Symposium Excursion Guide Geological Survey. Dept. of Mines and Energy, Sth. Aust.

Harte, B., and Hudson, N.F.C., 1979: Pelite facies series and the temperature and pressure of Dalradian metamorphism in E. Scotland. In: Harris, A.L., Holland, C.H., and Leake, B.E. (Eds.), The Caledonides of the British Isles - reviewed. Geol. Soc. London. Spec. Publ. No. 8: 323-337.

Harte, B., and Hudson, N.F.C., 1975: Determination of a pelite petrogenetic grid for thfe eastern Scottish Dalradian. Yearb. Carnegie Inst. Wash. 74: 438-446.

Hudson, N.F.C., 1986: Regional Metamorphism of Some Dalradian Pelites in the Buchan Area, NE Scotland. Contrib. Mineral Petrol. Vol. 73: 39-51.

Hollister, L.S., Grisson, G.C., Peters, E.K., Stowell, H.H., and Sisson, V.B., 1987: Confirmation of the empirical correlation of A1 in hornblende with pressures of solidification of calc-alkaline plutons. American Mineralogist, Vol. 72: 231-239.

Jenkins, R.J.F., in press: The Adelaide Fold Belt: Tectonic Reappraisal.

Kleeman, A.W.,1955: A reconnaissance of the structural petrology of the Mount Lofty Ranges. PhD thesis, Adelaide University (unpubl.).

Kneller, B.C., and Leslie, A.G., 1984: Amphibolite facies metamorphism in shear zones of the Buchan area of NE Scotland. J. meta. Geol. Vol. 2: 83-94.

Mancktelow, N.S., 1979: The structure and metamorphism of the Adelaide Fold Belt. PhD thesis, University of Adelaide (unpubl.).

Markham, N.L., 1951: Geology of Springton-Cambrai area. Hons. thesis, University of Adelaide (unpubl.).

Mehnert, K.R., 1971: Migmaites and the Origin of Granitic Rocks (2nd edn). Elsevier, New York.

Mills, K.J., 1973: The structural geology of the Warren National Park and the western portion of the Mount Crawford State Forest, South Australia. R.Soc.S.Aust., Trans.97: 281-296.

Mills, K.J., 1964: The structural geology of an area east of Springton, South Australia. PhD thesis, University of Adelaide (unpubl.).

Milnes, A.R., 1982: The Encounter Bay granites and their relationship to the Kanmantoo Group. In: Oliver, R.L. and Gatehouse, C.G. (eds): Guide to Excursions B1, B2, B3, B4, Geology of the Adelaide region, 16-29; Fourth International Symposium on Antarctic Earth Sciences.

Milnes, A.R., Compston, W., and Daily, B., 1977: Pre- to Syn tectonic emplacement of early Paleozoic granites in south-eastern South Australia. J. Geol. Soc. Aust. 24: 87-100.

Miyashiro, A., 1973: Paired and unpaired metamorphic belts. Tectonophysics 17: 241-254.

Oba, T., 1980: Phase relations in tbe tremolite-pargasite join. Contrib. Mineral Petrol 71: 246-256.

Offler, R., 1963: The structure and metamorphism of the Pewsley Vale area, north east of Williamstown, South Australia. PhD thesis, University of Adelaide (unpubl.).

Offler, R., and Fleming, P.D., 1968: A synthesis of folding and metamorphism in the Mt. Lofty Ranges, South Australia. J. Geol. Soc. Aust., 15: 245-265.

Pearce, J.A., Harris, N.B.W., and Tindle, A.G., 1984: Trace element discrimination diagrams for the tectonic interpretation of granitic rocks. Journal of Petrology 25, part 4: 956-983.

Pitcher, W.S., 1982: Granite type and tectonic environment. In: Hsu, K.J., (ed): Mountain Building Processes. Acedemic Press, London, pp.19-40.

Powell, R., and Smith, F.W., 1973: Pressure-temperature estimates for a late Dalradian Scottish event. Nature. Phys. Sci. Lond. 244: 70-71.

Preiss, W.V., (Compiler), 1987: The Adelaide Geosyncline - late Proterozoic stratigraphy sedimentation, palaeontology and tectonics. Geological Survey of South Australia Bulletin 53: 438pp.

Rattigan, J.H. and Wegener, C.F., 1951: Granites of the Palmer area and associated granitized sediments. Trans.R.Soc.S.Aust., 74: 149-164.

Richardson, S.W., and Powell, R., 1976: Thermal causes of the Dalradian metamorphism in the cenrtral Highlands of Scotland. Scott. J. Geol. 12, (3): 237-268.

Sandiford, M., Oliver, R.L., Mills, K.J., and Allen, R.V., A Cordierite-Staurolite-Muscovite Association, East of Springton, Mt. Lofty Ranges; Implications for the Metamorphic Evolution of the Kanmantoo Group. In press Geol. Soc. Aust. Spec. Pub. Daily Volume.

Shackleton, R.M., and Ries, A.C., 1984: The relation between regionally consistent stretching lineations and plate motions. Journal of Structural Geology, Vol. 6, No. 1/2:111-117.

Spear, F.S., 1981: Amphibole- Plagioclase Equilibria: An Empirical Model for the Relation Albite and Tremolite = Edenite + 4 Quartz. Contrib. Mineral.Petrol.,77: 355-364.

Sprigg, R.C. and Campana, B., 1953: The age and facies of the Kanmantoo Group, Eastern Mount Lofty Ranges and Kangaroo Island, South Australia. Aust.J.Sci., 16: 12-14.

Thomson, B.F., 1970: A review of the Precambrian and lower Palaeozoic tectonics of South Austraila. Trans.R.Soc.S.Aust., 94: 193-221.

Turner, S.P., 1986: Early Palaeozoic plutonism in western Victoria and eastern South Australia: Implications. Hons. thesis, University of Adelaide (unpubl.).

Wells, P.R.A., and Richardson, S.W., 1979: Thermal evolution of metamorphic rocks in the Central Highlands of Scotland. In: Harris, A.L., Holland, C.H., and Leake, B.E., (Eds.), The Caledonides of the British Isles - reviewed. Geol. Soc. London Spec. Publ. No. 8: 339-343.

White, A.J.R., 1966: Petrology and Structure of the Rathjen Granitic Gneiss of the Palmer Region, South Australia. J. Geol. Soc.Aust.,.Vol. 13: 471-489.

Winchester, J.A., 1974: The zonal pattern of regional metamorphism in the Scottish Caledonides. Journal Geol. Soc. London 130: 509-524.

REFERENCES

Kleeman, A.W. and Skinner, B.J..1959. The Kanmantoo Group in the Strathalbyn-Harrowgate region, South Australia. Trans.R.Soc.S.Aust., 82: 61-71.

Marlow, P.C. and Etheridge, M.A. 1977. Development of a layered crenulation cleavage in mica schists of the Kanmantoo Group near Maccelesfield, South Australia. Bull.geol.Soc.Am.,88: 873-882.

McKirdy, D.M., Sumartojo, J., Tucker, D.H. and Gostin, V. 1975. Organic, mineralogic and magnetic indications of metamorphism in the Tapley Hill Formation, Adelaide Geosyncline. Precambr.Res., 2: 345-373.

Mills, K.J., 1963. The geology of the Mount Crawford Granitic Gneiss and adjacent metasediments. Trans.R.Soc.S.Aust., 87: 167-183.

Talbot, J.L., 1964. The structural geometry of rocks of the Torrens Group near Adelaide, South Australia. J.geol.Soc.Aust., 11:33-48.

SAMPLE LOCALITY MAP

All samples prefixed by 898-

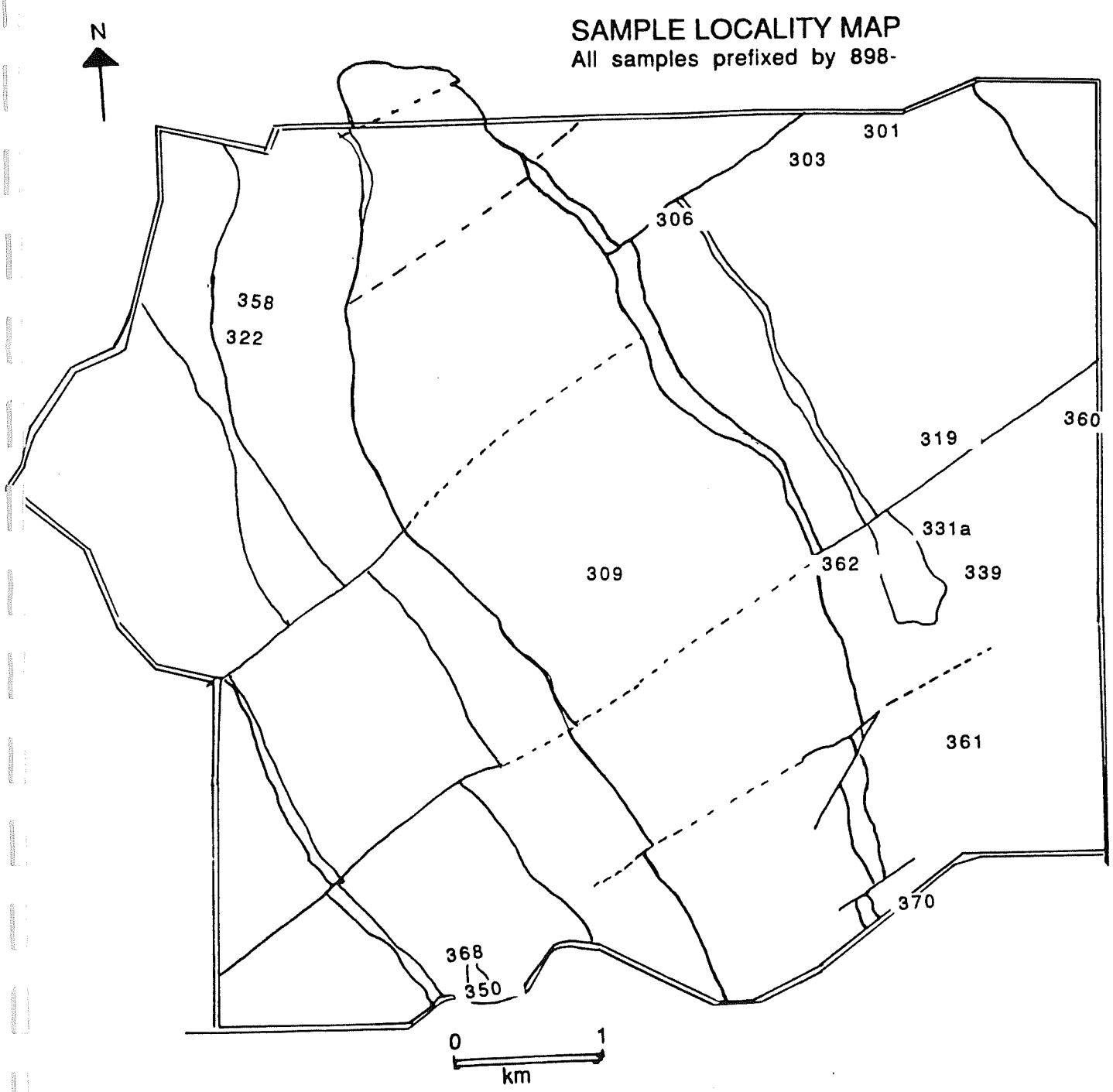

APPENDIX 1

SELECTED THIN SECTION DESCRIPTIONS

Sample 898-301

Sample 898-301 is an epidote aplite from the corner of Cook Hills Road.It is faulted against the epidote gneiss and intruded into the biotite schist. It is a medium grained, holocrystalline felsic rock, with no preferental alignment of minerals. Quartz forms deccusate crystal, is poikiloblastic with fluid inclusions. Plagioclase has fine albite twinning, is subhedral in form, inclined extinction with an extinction angle of 21°. It is biaxial positive with a 2V of 70° and is andesine. Potassium feldspar is orthoclase. It is biaxial negative with a 2V of 50°. Epidote shows blue and yellow diachronous birefringence and is erelatively abundant. Accessory minerals include biotite, deep red diamond-shaped sphene and muscovite. Modal proportions of the minerals are:

quartz	40 %
plagioclase	30 %
K-feldspar	25 %
biotite	4 %
accesories	1 %

Sample 898-303

Sample 898-303 is an epidote biotite gneiss from the Cook Hill Road paddock. It is intruding the calc silicate and the biotite schist. It is a medium to coarse grained holocrystalline, hypidomorphic textured rock composed of quartz and orthoclase with minor biotite, amphibole and epidote. Quartz is abundant as phenocrysts and as mossaic grains surrounding phenocrysts. This is indicative of them being products of recrystallization. Grains are subhedral to euhedral. Potassium feldspar is biaxial negativeand is orthoclase. It forms phenocrysts that are rimmed by re-equilibrated quartz. Plagioclase is restricted to the medium grained groundmass and has a rough preferred orientation to it. Crystals are subhedral, have inclined extinction and are andesine. The amphibole present is actinolite and has water green pleochroism, is biaxial positive and is poikiloblastic with semicircular grain boundry irregularities. Biotite shows rough preferred orientation. Accessory minerals inclued diamond-shaped sphene, epidote and magnetite. Modal proportions of the minerals are:

quartz	40 %
plagioclase	35 %
K-feldspar	15 %
biotite	10 %
amphibole	4 %
accessories	1 %

Sample 898-306

Sample 898-306 is a leucogabbro from Parker Road.Intruded parrallel to strike between the biotite schist and the epidote gneiss to the eastern side of the major syncline. It is a mafic rock, holocrystalline, generally coarse grained with laths up to 5 cm in length within a medium grained matrix. Amphiboles have a fibrous to silky texture and a random orientation. The amphibole is of a linear nature, fibrous texture, monoclinic extinction, biaxial positive with a 2V of 70° . It has high relief and pleochroic colours are white, pale yellow and water green. It is identified through its optics and with confirmation through microprobe data as Ca-rich actinolite. Potassium feldspar is microcline and has an average grainsize of 2mm. Grains are generally subhedral to euhedral and show perthitic texture. Plagioclase is monoclinic, biaxial with albite twinning. Probe data gives it composition of (Ab_{90}). Grainsize is on average 2mm and range from subhedral to euhedral in character. Accessory minerals include ilmenite and rutile. Modal proportions of the minerals are:

amphibole 56%
plagioclase 40%
accessories 4%

Sample 898-309

Sample 898-309 is Rathjen gneiss from Burns Road and is a coarse grained, lineated, foliated granitic gneiss. Quartz has triple point re-equilibrated grain boundaries Plagioclase is biaxial positive, has an extinction angle of 25° and a 2V of 70°. It shows albite twinning and is compositionally oligioclase. Potassium feldspar is orthoclase, is biaxial negative and a 2V of 50°. The amphibole has pleochroic colours of light green, emerald green and dark green, is biaxial negative with extinction angles of 25°. It is identified as hornblende and shows preferential alignment. as does biotite Accessory minerals include magnetite and tourmaline. Modal proportions of the minerals are:

quartz	20 %
plagioclase	30 %
K-feldspar	15 %
biotite	20 %
amphibole	10 %
accessories	5 %

Sample 895-319

Sample 898-319 is a calc silicate gneiss from Burns Road. It is conformable with the biotite schist and the albitized phyllite. A predominately felsic metasediment, hypidioblastic in texture it is porphyroblastic with preferred orientation of the ferromagnesiam minerals and irregular gneissic banding. Plagioclase has albite twinning, is biaxial positive with a 2V of 75° and an extinction angle of 32°. It occurs as small polygonal grains and is albite to oligioclase in composition. Quartz forms polygonal, small grains often surrounding the porphyroblasts with undulose extinction. Scapolite occurs as large crystals with inclusions of hornblende and diopside and has a poikiloblastic texture. It is biaxial negative with a 45° extinction angles. The amphibole present in this rock is biaxial positive, 2V of 75°, has pleochroic colours of white, yellow and water green. It occurs as laths and is subhedral, often having semicircular irregularities along grain edges and is actinolite. The pyroxene present occurs in equilibrium with scapolite and is heavily weathered to sericite. It is monoclinic, biaxial positive and has middle order interference colours and is diopside.Accessory minerals and opaques include rutile and diamond shaped sphene. Modal proportions of the minerals are:

scapolite	10 %
diopside	10 %
plagioclase	30 %
quartz	40 %
amphibole	7 %
accesories	3 %

Sample 898-331a

Sample 898-331a is an albitized phyllite from Burns Road conformable with the the calcsilicate gneiss. It is sugary in texture due to the albitization and often forms a amphibole rich sheet that peels off when weathered. Quartz occurs as porphyroblasts, with undulose extinction. It forms a polygonal, triple point boundaries. Plagioclase is albite, is poikiloblastic in texture and occurs as needle shaped or euhedral crystals and gives the rock its sugary

nature. It has a preferred orientation and is biaxial positive. Potassium feldspar is orthoclase, is biaxial negative with a 2V less than 40°. It is deccusate in form and is often include in plagioclase porphyroblasts. Biotite is scarce and is subhedral. The amphibole is actinolite, is biaxial negative, has a 2V of 30° and is preferrentially aligned. Accessory minerals include rutile and ilmenite. Modal proportions of the minerals are:

kspar	40 %
quartz	9 %
plagioclase	30 %
amphibole	30 %
accessories	1 %

Sample 898-350

Sample 898-350 is a gabbronorite from the Swan Reach Road intruded into the biotite gneiss on the western side of the syncline. It is coarse grained, holocrystalline with a hypidiomorphic texture. The amphibole in this rock varies in compositions. It makes up most of the ground mass and is sub to anhedral in form. It is biaxial negative with inclined extinction. It is identified as hornblende. The plagioclase is of two compositional varieties, is hypidiomorphic and forms zoned laths of euhedral to subhedral form. They are biaxial positive with inclined extinction and varying extinction angles. Probe data indicate that the cores are of a bytownite compositon with calcium percentages around 80% whilst the rims are of andesine/labradorite composition with calcium percentages dropping to 45%. Pyroxene is of two varieties, orthoclinic and monoclinic and show exsolution between the two. The orthoclinic pyroxene is hypersthene with monoclinic augite lamellae. This lamellae is detected by electron microprobe and not by a transmitted light. Accessory minerals include unexsolved magnetite and ilmenite along with apatite and sphene. Modal proportions of the minerals are:

amphibole	65 %
plagioclase	20 %
pyroxene	10 %
accessories	5 %

Sample 898-358

Sample 898-358 is an amphibolite dyke from Racetrack Road intruded between the calc silicate gneiss and the epidote gneiss on Racetrack Road. The amphibole in this specimen

is monoclinic, biaxial negative with pleochroic colours of dark emerald green, moss green and light green. It has a 2V of 30° and crystals are ribbons and lattice form. Probing has confirmed that this amphibole is hornblende. Relict igneous pyroxene is biaxial negative and is identified as augite. Quartz is slightly elongate with undulose extinction . Plagioclase is oligioclase, is elongate and also shows undulose extinction. Potassium feldspar is orthoclase and shows extensive kaolinization It is biaxial negative and has a 2V of 60°. Accessory minerals and opaques include rutile and magnetite. Modal proportions of the minerals are;

amphibole	60%
pyroxene	5%
feldspar	20%
quartz	10%
opaques	5%

Sample 898-361

Sample 898-361 is a talc gneiss from a track off the main Mt Pleasant/Swan Reach Road occuring in a small outcrop between the biotite schist and the calcsilicate gneiss. It is a talc bearing, medium to coarse grained quartzo-feldspathic rock which has a nodular outcrop form. The talc occurs as greenish radiating masses, is greasy to touch and is extensive throughout the rock and weathers to look like sillimanite in outcrop. Quartz is scarce in the rock and when it occurs it is small and forms a mossaic with the feldspars. Plagioclase is present as large laths and as small euhedral mossaic grains. It has albite twinning and and extinction angles of 25°. It is biaxial positive and is oligioclase. Potassium feldspar is present as large, tabular laths. They are poikiloblastic, subhedral and show replacement by talc in the form of ribbons and blebs. Crystal boundaries also show replacement by talc. It is biaxial negative and is orthoclase. Talc occurs as radiating, foliated groups, is biaxial negative with a 2V of 10°. It has high birefringence, second to third order colours and is not pleochroic. Accessory minerals include biotite, ilmenite and very large rutile crystals. Modal proportions of the minerals are;

quartz	25 %
plagioclase	25 %
K-feldspar	15 %
talc	30 %
accessories	5 %

Sample 898-362

Sample 898-362 biotite sillimanite schist from creek crossing Burns road to the east of the fold axis It often has coarse to pegmatitic layers of felsic material bordered by mafic selvages indicating a melt fraction. Percentages of micas to quartzo-feldspathic minerals are variable throughout the area and therefore becomes more felsic with gneissic banding. Quartz grains are subhedral and often show polygonal grain boundaries with undulose extinction. In leucacratic layers, it forms larger crystals, is porphyroblastic and has fluid inclusions. Plagioclase has albite twinning, is biaxial positive and an extinction angle of 20°. It sometimes occurs as fibres of albite as well as subhedral crystals.It also occurs as porphyroblasts and is slightly antiperthitic in texture. Potassium feldspar (orthoclase) is subhedral, biaxial negative and occurs as small aggrgates with other felsic mineral. Biotite has preferred orientation that tapers around aggregates of felsic minerals and has halos which are the result of radioactive decay. It is pleochroic and the colours are brown and olive green. Chlorite is also found in association with biotite and the two show relacement relationships.Sillimanite forms needle like laths and shows preferred orientation Accessory minerals and opaques include rutile which is amber, ilmenite which is black and an iron rich oxide which is magnetite. Modal proportions of the minerals are;

biotite	40 to 50 %
quartz	5 to 40 %
plagioclase	10 %
K-feldspar	20 %
sillimanite	5 to 40 %
opaques	1 %
oxides	4%

Sample 898-368

Sample 898-368 is a porphyritic gabbronorite on the main Mt Pleasant/Swan Reach Road, intruded between the biotite gneiss to the west of the syncline, along strike from unaltered equivalent. It is a basic rock, holocrystalline of medium grain size with some plagioclase laths becoming coarse to very coarse. It has a hypidiomorphic texture and is distinguished from its unaltered equivalent by the porphyritic nature of feldspar development and by the reduced grainsize. Quartz is euhedral and scarce. It is colourless but contains fluid

inclusions when it occurs as phenocrysts. Plagioclase forms phenocrysts and is rimmed by a mossaic of re-equilibrated plagioclase. Cores are bytownite and rims are andesine. The phenocrysts are subhedral, tabular laths up to 2cm in size, have multiple and simple twinning and are often zoned. They are biaxial positive. The cores show poilkioblastic development and have ribbons and rods of amphiboles included. They are often cracked and have a consertal intergrowth texture. Sericitation of the cores has often taken place. The rims are euhdral and show no evidence of cracking or of amphibole intergrowths. Amphibole constitutes most of the rock, is subhedral and forms the finer matix. It is monoclinic, biaxial negative with a 2V of 30°. It is subhedral and is pleochroic with colours of yellow ,green and emerald green. From optical and subsequent probe analysis this amphibole is identified as hornblende. Pyroxene has been uralitzed to a certain extent and shows recrystallization to the amphibole. Most of the pyroxene is orthorhombic and is biaxial negative. It is of a hypersthene composition. Clinopyroxene is probably present also is biaxial positive and is of an augite composition. Accessory minerals include ilmenite, rutile and magnetite.

Percentages are ;

amphibole	63%
pyroxene	9%
feldspar	20%
quartz	3%
accessories	5%

APPENDIX 2

SELECTIVE ELECTRON MICROPROBE DATA

Polished thin sections were coated with 250 um of carbon. Analysis of minerals was accomplished by using a KEVEX 7000 Series energy dispersive system which was attached to a JEOL 733 analyser.

All analysis was carried out under 15 KV accelerating voltage and 5 nA electron beam current. Data was then collected using PIBS style software. Calibration of the system was done using pure copper as a primary standard.

Detection limits for analysed elements are presented below.

ELEMENT	DETECTION LIMIT (wt %)
Na_2O	0.0511
MgO	0.0517
Al_2O_3	0.0590
SiO_2	0.0623
P_2O_3	0.0750
SO_3	0.1037
Cl	0.0406
Fe_2O_3	0.0072
K_2O	0.0565
CaO	0.0737
TiO_2	0.1191
V_2O_3	0.1216
Cr_2O_3	0.1366
MnO	0.1435
FeO	0.1634
NiO	0.2421
F	0.0479 - 0.0870

SAMPLES ANALYSED

898-306	Leucogabbro
898-309	Rathjen gneiss
898-319	Calcsilicate gneiss
898-322	Epidote gneiss
898-339	Calcsilicate gneiss
898-350	Gabbronorite
898-358	Amphibolite
898-360a	Migmatite mesosome

898-360b	Migmatite leucosome
898-360c	Migmatie mesosome
898-362	Sillimanite/biotite schist
898-368	Porphyritic gabbronorite
898-370	Migmatite

AMPHIBOLE DATA

Structural formulae based on 23 oxygen per formula unit and recalculated by Mac. intosh Excel program, Minchem II. X(Na) and v(a) were calculated as indicated in text (Chapter 6).

SiO2	58.08	55.50	57.91	58.60	58.43
TiO2					
Al2O3	0.64	1.95	0.90	0.62	0.59
Fe2O3					
FeO	6.93	7.01	7.73	6.98	6.77
MnO					
MgO	19.47	16.15	18.99	20.15	19.79
CaO	12.71	9.88	12.39	12.07	12.38
Na2O	0.45	0.69	0.73	0.88	0.46
K2O			0.12	0.10	
Total	98.3	91.2	98.8	99.4	98.4
Si	8.040	8.202	8.012	8.022	8.058
Ti	0.000	0.000	0.000	0.000	0.000
Al	0.104	0.340	0.147	0.100	0.096
Fe3+	0.000	0.000	0.000	0.000	0.000
Fe2+	0.802	0.866	0.894	0.799	0.781
Mn	0.000	0.000	0.000	0.000	0.000
Mg	4.017	3.557	3.916	4.111	4.068
Ca	1.885	1.564	1.837	1.770	1.829
Na	0.121	0.198	0.196	0.234	0.123
K	0.000	0.000	0.021	0.017	0.000
Total	14.969	14.727	15.023	15.054	14.955
v(a)	0.8792	0.8023	0.783	0.749	0.877
X(Na)	0.1208	0.1977	0.2001	0.2377	0.123

SiO2	45.22	43.4	44.31
TiO2	0.07	0.96	0.51
Al2O3	9.03	10.93	10.39
Fe2O3			
FeO	16.3	15.17	15.96
MnO		0.21	0.1
MgO	11.5	10.36	11.13
CaO	11.63	11.58	11.62
Na2O	1.96	1.32	1.45
K2O	0.39	1.08	0.77
Total	96.1	95.01	96.24
Si	6.847	6.643	6.699
Ti	0.008	0.111	0.058
Al	1.612	1.972	1.852
Fe3+	0	0	0
Fe2+	2.064	1.942	2.018
Mn	0	0.027	0.013
Mg	2.595	2.363	2.508
Ca	1.887	1.899	1.882
Na	0.575	0.392	0.425
K	0.075	0.211	0.149
Total	15.66	15.56	15.6

898-319 amphiboles

SiO2	58.88	54.89	51.77
TiO2	0.31	0.23	0.12
Al2O3	2.85	2.78	2.62
Fe2O3			
FeO	9.79	10.16	9.34
MnO	0.25	0.36	0.19
MgO	16.46	17.24	16.14
CaO	11.90	11.93	11.42
Na2O	0.95	0.97	0.79
K2O	0.10	0.09	
Total	101.5	98.7	92.4
Si	7.969	7.730	7.763
Ti	0.032	0.024	0.014
Al	0.455	0.462	0.463
Fe3+	0.000	0.000	0.000
Fe2+	1.108	1.197	1.171
Mn	0.029	0.043	0.024
Mg	3.320	3.618	3.607
Ca	1.726	1.800	1.835
Na	0.249	0.265	0.230
K	0.017	0.016	0.000
Total	14.905	15.155	15.107
v(a)	0.7334	0.719	0.7703
X(Na)	0.2537	0.2692	0.2297

898-350 amphiboles

SiO2	52.01	50.69	40.31	49.80
TiO2	0.33	0.26	1.43	
Al2O3	3.08	2.15	11.91	0.45
Fe2O3				
FeO	9.15	17.04	18.98	28.62
MnO	0.19	0.35	0.18	0.68
MgO	15.87	14.95	7.71	15.92
CaO	17.38	11.09	11.05	0.85
Na2O	0.51	0.53	1.79	0.17
K2O			1.11	
Total	98.5	97.1	94.5	96.5
Si	7.451	7.532	6.366	7.651
Ti	0.036	0.029	0.170	0.000
Al	0.520	0.377	2.218	0.082
Fe3+	0.000	0.000	0.000	0.000
Fe2+	1.096	2.117	2.507	3.677
Mn	0.023	0.044	0.024	0.088
Mg	3.388	3.310	1.815	3.645
Ca	2.668	1.766	1.870	0.140
Na	0.142	0.153	0.548	0.051
K	0.000	0.000	0.224	0.000
Total	15.324	15.327	15.741	15.334
v(a)	0.8583	0.8473	0.2282	0.9494
X(Na)	0.1417	0.1527	0.706	0.0506

898-358 amphiboles

SiO2	45.22	45.85	45.31	44.13	44.43	44.41
TiO2	0.57	0.56	0.48	0.57	0.61	0.65
Al2O3	8.53	8.54	8.89	9.12	9.31	9.45
Fe2O3						
FeO	16.40	16.41	16.37	16.31	16.88	16.84
MnO		0.13		0.20	0.29	0.18
MgO	11.40	11.34	11.17	10.99	10.95	10.95
CaO	11.84	11.94	11.87	11.87	11.82	11.91
Na2O	1.75	1.82	1.87	1.99	1.88	1.96
K2O	0.28	0.46	0.23	0.37	0.46	0.49
Total	96.0	97.1	96.2	95.6	96.6	96.8
Si	6.858	6.882	6.853	6.752	6.736	6.718
Ti	0.065	0.063	0.055	0.066	0.070	0.074
Al	1.525	1.511	1.585	1.645	1.664	1.685
Fe3+	0.000	0.000	0.000	0.000	0.000	0.000
Fe2+	2.080	2.060	2.071	2.087	2.140	2.131
Mn	0.000	0.017	0.000	0.026	0.037	0.023
Mg	2.577	2.537	2.518	2.506	2.474	2.469
Ca	1.924	1.920	1.924	1.946	1.920	1.931
Na	0.515	0.530	0.548	0.590	0.553	0.575
K	0.054	0.088	0.044	0.072	0.089	0.095
Total	15.598	15.608	15.597	15.691	15.683	15.700
v(a)	0.431	0.382	0.407	0.337	0.358	0.331
X(Na)	0.544	0.581	0.574	0.636	0.607	0.635

898-368a amphiboles

SiO2	49.27	45.20	43.43	45.26	46.26	49.39
TiO2	0.31	0.63	0.93	0.53	0.60	0.37
Al2O3	6.20	8.29	10.84	8.10	8.64	6.48
Fe2O3						
FeO	12.58	15.02	15.38	13.50	14.69	13.45
MnO	0.26	0.18	0.12	0.14	0.21	0.17
MgO	13.86	12.05	10.36	11.69	12.04	13.84
CaO	11.81	11.58	11.74	11.85	11.89	12.09
Na2O	0.82	1.22	1.32	1.10	1.33	0.95
K2O	0.43	0.74	1.08	0.61	0.67	0.47
Total	95.5	94.9	95.2	92.8	96.3	97.2
Si	7.307	6.897	6.642	7.004	6.929	7.236
Ti	0.035	0.072	0.107	0.062	0.068	0.041
Al	1.084	1.491	1.955	1.478	1.526	1.119
Fe3+	0.000	0.000	0.000	0.000	0.000	0.000
Fe2+	1.560	1.917	1.967	1.747	1.840	1.648
Mn	0.033	0.023	0.016	0.018	0.027	0.021
Mg	3.063	2.740	2.361	2.696	2.687	3.022
Ca	1.877	1.893	1.924	1.965	1.908	1.898
Na	0.236	0.361	0.391	0.330	0.386	0.270
K	0.081	0.144	0.211	0.120	0.128	0.088
Total	15.275	15.538	15.574	15.421	15.498	15.343
v(a)	0.683	0.495	0.398	0.550	0.486	0.642
X(Na)	0.257	0.422	0.496	0.375	0.443	0.296

SiO2	46.99	47.58	46.73	46.58	46.73	46.90
TiO2	0.63	0.62	0.74	0.80	0.67	0.59
Al2O3	8.77	8.54	9.17	9.53	9.16	9.00
Fe2O3						
FeO	14.85	14.54	15.13	14.33	14.85	14.64
MnO	0.16	0.18	0.24	0.22		0.32
MgO	11.71	11.93	11.39	11.58	11.49	11.51
CaO	12.39	12.46	12.25	12.26	12.23	12.35
Na2O	1.09	0.99	1.04	1.24	1.16	1.04
K2O	0.83	0.76	0.34	0.85	0.82	0.80
Total	97.4	97.6	97.0	97.4	97.1	97.2
Si	6.959	7.011	6.935	6.888	6.936	6.958
Ti	0.070	0.069	0.083	0.089	0.075	0.066
Al	1.531	1.484	1.604	1.662	1.603	1.574
Fe3+	0.000	0.000	0.000	0.000	0.000	0.000
Fe2+	1.839	1.792	1.878	1.772	1.843	1.817
Mn	0.020	0.022	0.030	0.028	0.000	0.040
Mg	2.585	2.620	2.519	2.552	2.542	2.545
Ca	1.966	1.967	1.948	1.943	1.945	1.963
Na	0.313	0.283	0.299	0.356	0.334	0.299
K	0.157	0.143	0.064	0.160	0.155	0.151
Total	15.440	15.391	15.362	15.450	15.433	15.414
v(a)	0.5302	0.5743	0.6363	0.4841	0.5109	0.5494
X(Na)	0.3712	0.33	0.3199	0.4235	0.3952	0.3526

PLAGIOCLASE DATA

Structural formulae based on 32 oxygen per formula unit and recalculated by Mac. intosh Excel program, Minchem II. X(Na) and v(a) were calculated as indicated in text (Chapter 6).

898-306 plagioclase

SiO2	69.72	68.50	70.11	69.63	68.11
Al2O3	20.17	19.85	19.65	19.53	19.07
CaO	0.31	0.57	0.74		0.46
Na2O	11.20	11.37	10.81	11.27	11.24
K2O	0.09	0.10	0.14		0.07
Total	101.5	100.4	101.5	100.4	99.0
Si	11.972	11.912	12.005	12.062	12.008
Al	4.083	4.069	3.967	3.989	3.964
Ca	0.057	0.106	0.136	0.000	0.087
Na	3.729	3.834	3.589	3.785	3.842
K	0.020	0.022	0.031	0.000	0.016
Total	19.861	19.943	19.727	19.836	19.916
X(Na)	0.980	0.968	0.956	1.000	0.974

898-309 plagioclase

SiO2	59.83	62.96	63.78
TiO2			
Al2O3	23.98	24.72	22.54
CaO	5.39	5.53	3.86
Na2O	6.94	8.70	9.31
K2O	0.40	0.15	0.35
Total	97.4	102.1	99.9
Si	10.887	10.944	11.280
Ti	0.000	0.000	0.000
Al	5.144	5.066	4.700
Ca	1.051	1.030	0.731
Na	2.448	2.932	3.193
K	0.093	0.033	0.079
Total	19.812	20.006	20.006

898-319 plagioclase

SiO2	67.87	67.21	67.70	67.87
Al2O3	21.11	21.27	21.59	21.19
CaO	1.86	1.92	2.09	1.93
Na2O	10.66	10.59	10.62	10.22
K2O	0.13	0.19	0.20	0.18
Total	101.6	101.2	102.2	101.4
Si	11.709	11.658	11.632	11.720
Al	4.294	4.350	4.373	4.314
Ca	0.344	0.357	0.385	0.357
Na	3.566	3.562	3.538	3.422
K	0.029	0.042	0.044	0.040
Total	19.941	19.969	19.972	19.853
X(Na)	0.905	0.899	0.892	0.896

898-350 plagioclase

SiO2	46.60	45.41	47.17	46.33	45.72	46.82	54.66	51.32	42.56	44.95	44.73	43.65
Al2O3	34.30	33.79	33.05	32.15	32.82	33.41	29.04	26.45	32.88	32.26	32.06	30.90
CaO	16.41	16.24	15.21	15.50	15.33	15.64	10.16	8.69	15.72	15.25	14.52	13.94
Na2O	2.28	2.13	3.01	2.77	2.89	2.66	5.93	6.18	2.00	3.74	2.84	2.65
K2O		0.14	0.07	0.16	0.17	0.10	0.14	0.15		0.30		
Total	99.6	97.7	98.5	96.9	96.9	98.6	99.9	92.8	93.2	96.5	94.2	91.1
Si	8.581	8.490	8.766	8.650	8.659	8.680	9.860	9.926	8.404	8.608	8.693	8.760
Al	7.446	7.448	7.241	7.077	7.328	7.303	6.176	6.031	7.655	7.283	7.345	7.311
Ca	3.238	3.253	3.029	3.101	3.111	3.107	1.964	1.801	3.326	3.129	3.024	2.998
Na	0.814	0.772	1.085	1.003	1.061	0.956	2.074	2.318	0.766	1.389	1.070	1.031
K	0.000	0.033	0.017	0.038	0.041	0.024	0.032	0.037	0.000	0.073	0.000	0.000
Total	20.080	19.996	20.137	19.869	20.200	20.070	20.105	20.113	20.151	20.482	20.132	20.100
X(Na)	0.201	0.190	0.263	0.242	0.252	0.234	0.510	0.558	0.187	0.302	0.261	0.256

898-358 plagioclase

SiO2	58.82	66.32	66.91	61.45	60.16	60.70	60.81	60.32	61.63
Al2O3	23.38	20.66	20.98	24.32	25.44	24.74	24.98	23.35	25.56
CaO	5.74	1.79	1.87	5.87	7.03	6.38	6.60	5.12	6.77
Na2O	7.98	10.28	10.26	8.01	7.36	7.59	7.78	7.15	7.75
K2O	0.20	0.09	0.09		0.07	0.17	0.14	0.21	0.12
Total	96.1	99.1	100.1	99.7	100.1	99.6	100.3	96.2	101.8
Si	10.850	11.718	11.705	10.910	10.694	10.805	10.771	10.960	10.759
Al	5.084	4.303	4.327	5.091	5.331	5.192	5.216	5.002	5.260
Ca	1.135	0.339	0.351	1.117	1.339	1.217	1.253	0.997	1.266
Na	2.854	3.522	3.480	2.758	2.537	2.620	2.672	2.519	2.623
K	0.047	0.020	0.020	0.000	0.016	0.039	0.032	0.049	0.027
Total	19.970	19.902	19.882	19.875	19.917	19.873	19.944	19.527	19.936
X(Na)	0.707	0.907	0.904	0.712	0.652	0.676	0.675	0.707	0.670

898-368 a plagioclase

SiO2	47.83	48.23	56.37	57.63	49.32	56.52	47.91	57.35
Al2O3	32.92	33.30	28.56	28.33	32.56	28.39	33.38	27.91
CaO	16.18	16.29	10.46	9.68	15.90	10.42	16.65	9.95
Na2O	2.39	2.40	5.74	6.16	2.70	5.74	2.43	6.00
K2O	0.06	0.09	0.21	0.25	0.13	0.17		0.20
Total	99.4	100.3	101.3	102.1	100.6	101.2	100.4	101.4
Si	8.818	8.778	10.013	10.140	8.909	10.032	8.729	10.158
Al	7.155	7.145	5.981	5.877	6.934	5.941	7.170	5.828
Ca	3.196	3.177	1.991	1.825	3.078	1.982	3.250	1.888
Na	0.854	0.847	1.977	2.102	0.946	1.975	0.858	2.061
K	0.014	0.021	0.048	0.056	0.030	0.038	0.000	0.045
Total	20.038	19.968	20.009	20.000	19.897	19.968	20.008	19.981
X(Na)	0.210	0.209	0.492	0.528	0.233	0.494	0.209	0.516

898-368 b plagioclase

SiO2	47.39	56.98	57.33	51.90	48.31	48.04	55.64	48.57	49.02	57.00	47.07	48.5
Al2O3	27.09	28.63	27.96	31.40	34.83	26.09	29.68	33.15	33.90	28.45	35.04	34.2
CaO	9.86	9.59	9.05	12.84	16.38	9.22	10.63	15.47	15.41	9.45	16.77	16.0
Na2O	5.26	6.39	6.90	4.53	2.77	5.30	5.88	3.09	3.14	6.67	2.39	2.6
K2O	0.18	0.16	0.18	0.08		0.13	0.16	0.10	0.12	0.19	0.12	0.0
Total	89.8	101.8	101.4	100.8	102.3	88.8	102.0	100.4	101.6	101.8	101.4	101.
Si	9.555	10.065	10.158	9.347	8.656	9.772	9.839	8.816	8.814	10.068	8.525	8.74
Al	6.439	5.962	5.840	6.667	7.357	6.257	6.188	7.094	7.186	5.924	7.481	7.27
Ca	2.130	1.815	1.718	2.478	3.145	2.010	2.014	3.009	2.969	1.788	3.254	3.10
Na	2.056	2.189	2.370	1.582	0.962	2.090	2.016	1.088	1.095	2.284	0.839	0.91
K	0.046	0.036	0.041	0.018	0.000	0.034	0.036	0.023	0.028	0.043	0.028	0.01
Total	20.226	20.066	20.128	20.092	20.120	20.162	20.093	20.029	20.090	20.107	20.128	20.05
X(Na)	0.486	0.542	0.574	0.388	0.234	0.506	0.496	0.264	0.268	0.555	0.204	0.22

BIOTITE DATA

Structural formulae based on 22 oxygen per formula unit and recalculated by Macintosh Excel program, Minchem II.

898-309 biotite

SiO2	37.00	36.67	36.59	37.69	37.00	37.04
TiO2	3.14	3.11	3.22	2.68	3.08	3.09
Al2O3	14.41	14.58	14.33	16.71	14.57	14.42
Fe2O3						
FeO	22.17	21.57	21.12	19.14	22.04	22.22
MnO	0.36	0.23	0.29	0.12	0.18	0.28
MgO	9.42	9.15	9.31	7.98	9.20	9.56
CaO						
Na2O			0.22	0.23	0.19	0.10
K2O	10.05	9.88	9.96	8.86	10.05	9.80
Total	96.6	95.2	95.0	93.4	96.3	96.5
Si	5.672	5.682	5.680	5.805	5.681	5.673
Ti	0.362	0.362	0.376	0.310	0.356	0.356
Al	2.604	2.664	2.623	3.034	2.637	2.604
Fe3+	0.000	0.000	0.000	0.000	0.000	0.000
Fe2+	2.843	2.795	2.742	2.465	2.830	2.846
Mn	0.047	0.030	0.038	0.016	0.023	0.036
Mg	2.152	2.113	2.154	1.832	2.105	2.182
Ca	0.000	0.000	0.000	0.000	0.000	0.000
Na	0.000	0.000	0.066	0.069	0.057	0.030
K	1.966	1.953	1.973	1.741	1.969	1.915
Total	15.646	15.600	15.652	15.272	15.657	15.642

898-360A biotite

SiO2	35.55	35.93	34.97	36.25	35.87	36.12	36.15	35.92	35.57	35.71	35.71	35.96
TiO2	2.91	2.57	2.93	2.91	2.71	2.95	2.66	3.14	2.71	2.84	2.84	2.84
Al2O3	17.57	18.13	17.89	18.52	17.78	18.01	17.93	17.96	17.70	18.16	18.16	18.04
Fe2O3												
FeO	17.20	17.08	16.51	16.93	17.38	17.23	16.42	16.68	17.20	16.72	16.72	17.06
MnO												
MgO	10.63	10.50	9.48	10.16	10.37	10.33	11.03	10.22	10.17	10.05	10.05	10.13
CaO												
Na2O	0.27		0.30	0.19	0.18	0.27		0.29	0.22	0.24	0.24	0.15
K2O	9.85	9.24	9.25	9.68	9.72	10.07	9.63	9.74	9.62	9.81	9.81	9.78
Total	94.0	93.5	91.3	94.6	94.0	95.0	93.8	94.0	93.2	93.5	93.5	94.0
Si	5.705	5.754	5.741	5.739	5.744	5.729	5.761	5.737	5.745	5.733	5.733	5.750
Ti	0.351	0.310	0.362	0.346	0.326	0.352	0.319	0.377	0.329	0.343	0.343	0.342
Al	3.324	3.423	3.462	3.456	3.357	3.368	3.369	3.382	3.370	3.437	3.437	3.401
Fe3+	0.000	0.000	0.000	0.000	0.000	0.000	0.000	0.000	0.000	0.000	0.000	0.000
Fe2+	2.308	2.288	2.267	2.241	2.328	2.285	2.188	2.228	2.323	2.245	2.245	2.281
Mn	0.000	0.000	0.000	0.000	0.000	0.000	0.000	0.000	0.000	0.000	0.000	0.000
Mg	2.542	2.506	2.319	2.397	2.475	2.442	2.620	2.433	2.448	2.405	2.405	2.414
Ca	0.000	0.000	0.000	0.000	0.000	0.000	0.000	0.000	0.000	0.000	0.000	0.000
Na	0.084	0.000	0.095	0.058	0.056	0.083	0.000	0.090	0.069	0.075	0.075	0.047
K	2.017	1.888	1.937	1.955	1.986	2.038	1.958	1.985	1.982	2.009	2.009	1.995
Total	16.332	16.169	16.183	16.193	16.272	16.296	16.215	16.232	16.266	16.247	16.247	16.229

898-360B biotite

SiO2	35.34	32.98	35.66	35.77	36.10	36.04	35.58	35.28
TiO2	2.44	2.75	2.57	2.55	2.60	2.72	2.62	2.52
Al2O3	17.62	16.03	17.55	17.93	17.46	18.02	17.47	17.47
Fe2O3								
FeO	16.03	14.92	16.44	15.80	16.31	16.45	15.79	15.51
MnO								
MgO	11.27	10.00	11.35	10.75	11.36	10.97	11.41	10.97
CaO								
Na2O	0.25	0.21	0.23	0.28	0.33	0.21	0.19	0.52
K2O	9.29	7.18	9.06	7.39	9.06	9.98	10.07	9.08
Total	92.2	84.1	92.9	90.5	93.2	94.4	93.1	91.4
Si	5.480	5.555	5.490	5.569	5.528	5.479	5.481	5.510
Ti	0.285	0.348	0.298	0.299	0.299	0.311	0.304	0.296
Al	3.221	3.183	3.186	3.291	3.152	3.230	3.173	3.217
Fe3+	0.000	0.000	0.000	0.000	0.000	0.000	0.000	0.000
Fe2+	2.079	2.102	2.117	2.057	2.089	2.091	2.034	2.026
Mn	0.000	0.000	0.000	0.000	0.000	0.000	0.000	0.000
Mg	2.604	2.510	2.604	2.494	2.593	2.485	2.620	2.553
Ca	0.000	0.000	0.000	0.000	0.000	0.000	0.000	0.000
Na	0.075	0.069	0.069	0.085	0.098	0.062	0.057	0.157
K	1.838	1.543	1.780	1.468	1.770	1.936	1.979	1.809
Total	15.582	15.311	15.543	15.263	15.530	15.594	15.647	15.569

898-360C biotite

SiO2	35.49	35.30	35.90	35.45	36.05	35.52	35.85	37.56	37.98	37.43
TiO2	2.76	2.82	2.66	2.96	2.80	2.68	2.54	3.01	2.56	2.92
Al2O3	17.71	17.86	17.71	17.42	18.00	18.00	18.56	19.04	19.06	18.30
Fe2O3										
FeO	17.02	17.32	17.17	17.19	17.46	16.67	16.55	17.44	18.10	17.15
MnO										
MgO	10.46	10.01	10.24	9.91	10.76	10.60	9.99	10.63	10.68	11.15
CaO										
Na2O		0.14	0.14		0.18			0.17		
K2O	9.84	9.86	10.01	9.86	9.22	9.48	9.41	10.27	10.10	10.18
Total	93.3	93.3	93.8	92.8	94.5	93.0	92.9	98.1	98.5	97.1
Si	5.726	5.707	5.764	5.758	5.725	5.725	5.763	5.742	5.785	5.775
Ti	0.335	0.343	0.321	0.362	0.334	0.325	0.307	0.346	0.293	0.339
Al	3.369	3.404	3.352	3.336	3.370	3.421	3.517	3.431	3.422	3.329
Fe3+	0.000	0.000	0.000	0.000	0.000	0.000	0.000	0.000	0.000	0.000
Fe2+	2.297	2.342	2.305	2.335	2.319	2.247	2.225	2.230	2.306	2.213
Mn	0.000	0.000	0.000	0.000	0.000	0.000	0.000	0.000	0.000	0.000
Mg	2.515	2.412	2.450	2.399	2.546	2.546	2.393	2.422	2.424	2.564
Ca	0.000	0.000	0.000	0.000	0.000	0.000	0.000	0.000	0.000	0.000
Na	0.000	0.044	0.044	0.000	0.055	0.000	0.000	0.050	0.000	0.000
K	2.026	2.034	2.050	2.043	1.868	1.950	1.930	2.003	1.963	2.004
Total	16.267	16.286	16.286	16.234	16.218	16.214	16.136	16.223	16.192	16.224

SiO2	35.98	35.68	35.99	35.98	35.56	36.00	36.05	35.94	36.80	36.26
TiO2	2.12	2.44	2.52	2.45	2.51	2.37	2.55	2.50	2.39	2.65
Al2O3	18.37	18.13	18.38	18.40	17.82	18.31	18.74	18.33	18.78	18.30
Fe2O3										
FeO	17.35	17.63	17.83	17.91	17.92	17.73	18.17	18.09	17.42	18.26
MnO										
MgO	10.53	10.09	10.64	10.74	10.42	10.66	10.84	10.90	10.84	10.80
CaO										
Na2O	0.42	0.42	0.49	0.49	0.52	0.54	0.60	0.64	0.66	0.54
K2O	9.27	9.42	9.37	9.19	9.24	9.47	9.47	9.47	9.46	9.55
Total	94.0	93.8	95.2	95.2	94.0	95.1		95.9	96.4	96.4
Si	5.491	5.478	5.442	5.440	5.458	5.454	5.393	5.412	5.478	5.432
Ti	0.243	0.282	0.287	0.279	0.290	0.270	0.287	0.283	0.268	0.299
Al	3.305	3.282	3.276	3.280	3.225	3.270	3.305	3.254	3.295	3.232
Fe3+	0.000	0.000	0.000	0.000	0.000	0.000	0.000	0.000	0.000	0.000
Fe2+	2.214	2.264	2.255	2.265	2.300	2.246	2.273	2.278	2.169	2.288
Mn	0.000	0.000	0.000	0.000	0.000	0.000	0.000	0.000	0.000	0.000
Mg	2.395	2.309	2.398	2.420	2.384	2.407	2.417	2.446	2.405	2.411
Ca	0.000	0.000	0.000	0.000	0.000	0.000	0.000	0.000	0.000	0.000
Na	0.124	0.125	0.144	0.144	0.155	0.159	0.174	0.187	0.190	0.157
K	1.805	1.845	1.808	1.773	1.810	1.830	1.808	1.819	1.796	1.825
Total	15.578	15.584	15.609	15.600	15.622	15.636	15.658	15.681	15.601	15.644

APPENDIX 3

GEOCHEMICAL METHODS

Sample Preparation

(1) Samples were crushed using departmental jaw crusher.

(2) These were ground into a fine powder using a Siebtechnic tungsten carbide mill.

(3) Powder of the samples were then ignited overnight at 960°; for each 280 mg of ignited samle, 20 mg of sodium nitrate and 1.5 g of flux were weighed out, mixed and used to produce a fused button.

(4) 5 g of unignited sample powder was used to produce pressed pellets for trace element analysis.

Major Element analyses

(1) SiO_2, Al_2O_3, Fe_2O_3, MnO, MgO, CaO, Na_2O, K_2O, TiO_2 and P_2O_5 concentrations were determined using the programmable Siemens S.R.S. X.R.D.

(2) Digestion of 50-60 mg of ignited sample in a teflon beaker containing 2 ml of sulphuric acid and 10 ml of hydrofluoric acid at 110° for a minimum of 12 hours to determine Na_2O concentrations. Each solution was made up to 100 ml with distilled water and the ultimate Na_2O concentration was then determined using the Varian Techtron Atomic Absorption Spectrophotometre.

Trace Element Analyses

(1) Sr, Rb, Zr, Nb, Ba, Sc, Ce, Nd, Cr, Ni, V, La, Ga abundances were determined by means of the Siemens X.R.F.

Results

All results are included in tables in the text.

APPENDIX 4

MAPS AND STRUCTURAL DATA

Readings

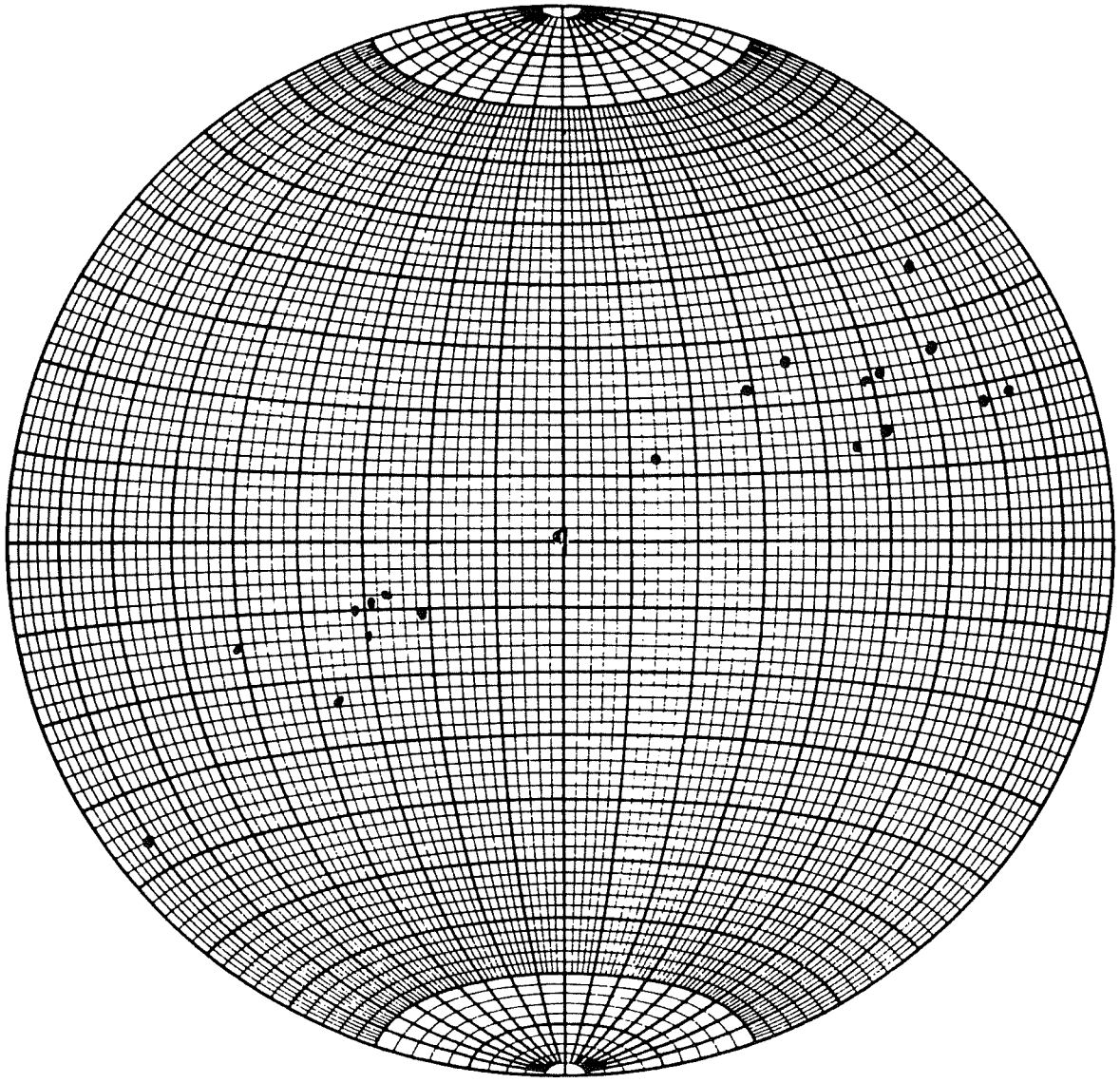

SCHMIDT NET